



ARCHIVIO ISTITUZIONALE  
DELLA RICERCA

Alma Mater Studiorum Università di Bologna  
Archivio istituzionale della ricerca

Sandy coastlines under threat of erosion

This is the final peer-reviewed author's accepted manuscript (postprint) of the following publication:

*Published Version:*

Sandy coastlines under threat of erosion / Vousdoukas M.I.; Ranasinghe R.; Mentaschi L.; Plomaritis T.A.; Athanasiou P.; Luijendijk A.; Feyen L.. - In: NATURE CLIMATE CHANGE. - ISSN 1758-678X. - ELETTRONICO. - 10:3(2020), pp. 260-263. [10.1038/s41558-020-0697-0]

This version is available at: <https://hdl.handle.net/11585/883737> since: 2022-05-02

*Published:*

DOI: <http://doi.org/10.1038/s41558-020-0697-0>

*Terms of use:*

Some rights reserved. The terms and conditions for the reuse of this version of the manuscript are specified in the publishing policy. For all terms of use and more information see the publisher's website.

(Article begins on next page)

This item was downloaded from IRIS Università di Bologna (<https://cris.unibo.it/>).  
When citing, please refer to the published version.

This is the final peer-reviewed accepted manuscript of:

Vousdoukas, M.I., Ranasinghe, R., Mentaschi, L. et al. *Sandy coastlines under threat of erosion*. Nat. Clim. Chang. 10, 260–263 (2020).

The final published version is available online at: <https://doi.org/10.1038/s41558-020-0697-0>

#### Rights / License:

The terms and conditions for the reuse of this version of the manuscript are specified in the publishing policy. For all terms of use and more information see the publisher's website.

This item was downloaded from IRIS Università di Bologna (<https://cris.unibo.it/>)

**When citing, please refer to the published version.**

1  
2

# 1. Extended Data

Figure #	Figure title	Filename	Figure Legend
Extended Data Fig. 1	Geographical regions considered in the present analysis	Vousdoukas_ED_01.eps	Geographical regions considered in the present analysis, based on the IPCC SREX report and limited to those that contain ice-free sandy coastlines
Extended Data Fig. 2	Projected long term shoreline change due to SLR driven retreat (R) alone, by the year 2050 and 2100 under RCP4.5 and RCP8.5.	Vousdoukas_ED_02.eps	Projected long term shoreline change due to SLR driven retreat (R) alone, by the year 2050 (a,c) and 2100 (b,d) under RCP4.5 (a-b) and RCP8.5 (c-d). Values represent the median change and positive/negative values express accretion/erosion in m, relative to 2010. The global average median change is shown in the inset text for each case, along with the 5 <sup>th</sup> -95 <sup>th</sup> percentile range.
Extended Data Fig. 3	Projected long term shoreline change driven due to the ambient shoreline change rate (AC) alone, by the year 2050 and 2100.	Vousdoukas_ED_03.eps	Projected long term shoreline change driven due to the ambient shoreline change rate (AC) alone, by the year 2050 (a) and 2100 (b). Values represent the median change and positive/negative values express accretion/erosion in m, relative to 2010. The global average median change is shown in the inset text for each case, along with the 5 <sup>th</sup> -95 <sup>th</sup> percentile range.
Extended Data Fig. 4	Projected change in 100-year episodic beach erosion for the year 2050 and 2100 under RCP4.5 and	Vousdoukas_ED_04.eps	Projected change in 100-year episodic beach erosion for the year 2050 (a,c) and 2100 (b,d) under RCP4.5 (a-b) and RCP8.5 (c-d). Values represent the median change and positive/negative values express less/more erosion (m), relative to 2010. The global average median change is shown in

	RCP8.5.		the inset text for each case, along with the 5 <sup>th</sup> -95 <sup>th</sup> percentile range.
Extended Data Fig. 5	Projected median long term shoreline change under RCP4.5 by the year 2050 ( $dx_{shore,LT}$ ), for the 26 IPCC SREX sub- regions and the worldwide average	Vousdoukas_ED_05.eps	Projected median long term shoreline change under RCP4.5 by the year 2050 ( $dx_{shore,LT}$ ), for the 26 IPCC SREX sub- regions and the worldwide average (horizontal bar plot; positive/negative values express accretion/erosion in m). Shoreline change is considered to be the result of SLR retreat (R) and ambient shoreline change trends (AC). Pie plots show the relative contributions of R and AC to the projected median $dx_{shore,LT}$ , with transparent patches expressing accretive trends. Vertical bar plots show the relative contributions of R and AC, as well as that of RCPs, to the total uncertainty in projected median $dx_{shore,LT}$ .
Extended Data Fig. 6	Projected median long term shoreline change under RCP8.5 by the year 2050 ( $dx_{shore,LT}$ ), for the 26 IPCC SREX sub- regions and the worldwide average	Vousdoukas_ED_06.eps	Projected median long term shoreline change under RCP8.5 by the year 2050 ( $dx_{shore,LT}$ ), for the 26 IPCC SREX sub- regions and the worldwide average (horizontal bar plot; positive/negative values express accretion/erosion in m). Shoreline change is considered to be the result of SLR retreat (R) and ambient shoreline change trends (AC). Pie plots show the relative contributions of R and AC to the projected median $dx_{shore,LT}$ , with transparent patches expressing accretive trends. Vertical bar plots show the relative contributions of R and AC, as well as that of RCPs, to the total uncertainty in projected median $dx_{shore,LT}$ .
Extended Data Fig. 7	Projected median long term shoreline change under RCP4.5 by the year 2100 ( $dx_{shore,LT}$ ), for the 26 IPCC SREX sub- regions and the worldwide average	Vousdoukas_ED_07.eps	Projected median long term shoreline change under RCP4.5 by the year 2100 ( $dx_{shore,LT}$ ), for the 26 IPCC SREX sub- regions and the worldwide average (horizontal bar plot; positive/negative values express accretion/erosion in m). Shoreline change is considered to be the result of SLR retreat (R) and ambient shoreline change trends (AC). Pie plots show the relative contributions of R and AC to the projected

			median $dx_{shore,LT}$ , with transparent patches expressing accretive trends. Vertical bar plots show the relative contributions of R and AC, as well as that of RCPs, to the total uncertainty in projected median $dx_{shore,LT}$ .
Extended Data Fig. 8	Percentage length of sandy beach shoreline that is projected to retreat by more than 50, 100 and 200 m per IPCC SREX sub-region	Vousdoukas_ED_08.eps	Bar plots showing, per IPCC SREX sub-region, the percentage length of sandy beach shoreline that is projected to retreat by more than 50 (blue), 100 (yellow) and 200 m (red), by 2050 (a,c) and 2100 (b,d), under RCP4.5 (a-b) and RCP8.5 (c-d) relative to 2010. Transparent color patches indicate the 5 <sup>th</sup> -95 <sup>th</sup> quantile range and solid rectangles show the median value. For the region abbreviations, please see Extended Data Fig. 1.
Extended Data Fig. 9	Length of sandy beach shoreline that is projected to retreat by more than 50, 100 and 200 m per IPCC SREX sub-region	Vousdoukas_ED_09.eps	Bar plots showing, per IPCC SREX sub-region, the length (in km) of sandy beach shoreline that is projected to retreat by more than 50 (blue), 100 (yellow) and 200 m (red), by 2050 (a,c) and 2100 (b,d), under RCP4.5 (a-b) and RCP8.5 (c-d) relative to 2010. Transparent color patches indicate the 5 <sup>th</sup> -95 <sup>th</sup> quantile range and solid rectangles show the median value. For the region abbreviations, please see Supplementary Figs. S2 and S5
Extended Data Fig. 10	Per country length of sandy beach shoreline that is projected to retreat by more than 100 m	Vousdoukas_ED_10.eps	Per country length of sandy beach coastline which is projected to retreat by more than 100 m by 2050 (a,c) and 2100 (b,d), under RCP4.5 (a-b) and RCP8.5 (c-d). Values are based on the median long term shoreline change, relative to 2010.

3 **2. Supplementary Information:**

4 **A. Flat Files**

5

Item	Present?	Filename	A brief, numerical description of file contents.
		This should be the	

		name the file is saved as when it is uploaded to our system, and should include the file extension. The extension must be .pdf	i.e.: <i>Supplementary Figures 1-4, Supplementary Discussion, and Supplementary Tables 1-4.</i>
Supplementary Information	Yes	Vousdoukas_NLetter_SI.pdf	<i>Supplementary Figure 1, Supplementary Tables 1-4.</i>
Reporting Summary	Choose an item.		

6  
7  
8  
9

## B. Additional Supplementary Files

Type	Number	Filename	Legend or Descriptive Caption
	If there are multiple files of the same type this should be the numerical indicator. i.e. "1" for Video 1, "2" for Video 2, etc.	This should be the name the file is saved as when it is uploaded to our system, and should include the file extension. i.e.: <i>Smith_Supplementary_Video_1.mov</i>	Describe the contents of the file
Choose an item.			
Choose an item.			
Choose an item.			
Choose an item.			
Choose an item.			
Choose an item.			

10  
11

## 3. Source Data

12  
13

Parent Figure or Table	Filename	Data description
	This should be the name the file is saved as when it is uploaded to	e.g.: Unprocessed Western Blots and/or gels,

	our system, and should include the file extension. i.e.: <i>Smith_SourceData_Fig1.xls</i> , or <i>Smith_Unmodified_Gels_Fig1.pdf</i>	Statistical Source Data, etc.
Source Data Fig. 1		
Source Data Fig. 2		
Source Data Fig. 3		
Source Data Fig. 4		
Source Data Fig. 5		
Source Data Fig. 6		
Source Data Fig. 7		
Source Data Fig. 8		
Source Data Extended Data Fig. 1		
Source Data Extended Data Fig. 2		
Source Data Extended Data Fig. 3		
Source Data Extended Data Fig. 4		
Source Data Extended Data Fig. 5		

Source Data Extended Data Fig. 6		
Source Data Extended Data Fig. 7		
Source Data Extended Data Fig. 8		
Source Data Extended Data Fig. 9		
Source Data Extended Data Fig. 10		

14

15

16

## Sandy coastlines under threat of erosion

17 Michalis I. Vousdoukas<sup>1\*</sup>, Roshanka Ranasinghe<sup>2,3,4</sup>, Lorenzo Mentaschi<sup>1</sup>, Theocharis A. Plomaritis<sup>5,6</sup>,  
18 Panagiotis Athanasiou<sup>3,4</sup>, Arjen Luijendijk<sup>4,7</sup>, Luc Feyen<sup>1</sup>

19 <sup>1</sup> European Commission, Joint Research Centre (JRC), Email: [Michail.VOUSDOKAS@ec.europa.eu](mailto:Michail.VOUSDOKAS@ec.europa.eu); Tel:  
20 +39 033278-6499; Fax: +39 033278-665

21 <sup>2</sup> Department of Water Science and Engineering, IHE Delft Institute for Water Education, PO Box 3015,  
22 2610 DA Delft, the Netherlands

23 <sup>3</sup> Water Engineering and Management, Faculty of Engineering Technology, University of Twente, PO, Box  
24 217, 7500 AE Enschede, the Netherlands

25 <sup>4</sup> Harbour, Coastal and Offshore Engineering, Deltares, PO Box 177, 2600 MH Delft, the Netherlands

26 <sup>5</sup> University of Cadiz, Dpt. Applied Physics, CASEM, University of Cadiz, 11510 Puerto Real, Cádiz, Spain

27 <sup>6</sup> CIMA, University of Algarve, Campus de Gambelas, 8005-139, Faro, Portugal

28 <sup>7</sup> Faculty of Civil Engineering and Geosciences, Department of Hydraulic Engineering, Delft University of  
29 Technology, P.O. Box 5048, 2600 GA Delft, The Netherlands



30

31 \*Corresponding author address:

32 Dr Michalis Vousdoukas

33 European Commission, Joint European Research Centre (JRC), Via Enrico Fermi 2749, I-21027, Ispra,

34 Italy. Email: [Michail.VOUSDOKAS@ec.europa.eu](mailto:Michail.VOUSDOKAS@ec.europa.eu); Tel: +39 033278-6499; Fax: +39 033278-665

35

36 **Sandy beaches occupy more than one third of the global coastline<sup>1</sup> and have high socio-**  
37 **economic value related to recreation, tourism, and ecosystem services<sup>2</sup>. Beaches are the interface**  
38 **between land and ocean, providing coastal protection from marine storms and cyclones<sup>3</sup>. However**  
39 **the presence of sandy beaches cannot be taken for granted, as they are under constant change, driven**  
40 **by meteorological<sup>4,5</sup>, geological<sup>6</sup>, and anthropogenic factors<sup>1,7</sup>. A substantial proportion of the world's**  
41 **sandy coastline is already eroding<sup>1,7</sup>, a situation that could be exacerbated by climate change<sup>8,9</sup>. Here,**  
42 **we show that with, climate mitigation, ambient trends in shoreline dynamics, combined with coastal**  
43 **recession driven by sea level rise could result in the near extinction of almost half of the world's sandy**  
44 **beaches by the end of the century. Moderate greenhouse gas emission mitigation could prevent 40%**  
45 **of shoreline retreat. Projected shoreline dynamics are dominated by sea level rise for the majority of**  
46 **sandy beaches, but in certain regions this is overshadowed by ambient shoreline changes. In West and**  
47 **East Asia, long-term accretion up to 200-300 m is projected. A significant proportion of the threatened**  
48 **sandy shorelines are in densely populated areas, underlining the need for the design and**  
49 **implementation of effective adaptive measures.**

50

51 The coastal zone is among the most developed areas worldwide, containing an abundance of  
52 developments, critical infrastructure<sup>10</sup>, and ecosystems<sup>2,3</sup>. As a result, population density tends to be  
53 higher near the coast<sup>11</sup>, and most projections indicate that current trends of coastward migration,  
54 urbanization and population growth will continue<sup>12,13</sup>. Of the different beach typologies found  
55 worldwide sandy beaches are the most heavily utilized<sup>14</sup> and are among the most geomorphologically  
56 complex, with the shoreline, i.e. the mean water line along the coast, changing constantly under forcing-  
57 response interactions between natural and anthropogenic factors<sup>7</sup>.

58 The global mean sea level has been increasing at an accelerated rate during the past 25 years<sup>15</sup> and will  
59 continue to do so in view of climate change<sup>16,17</sup>. While shoreline change can be the combined result of a  
60 wide range of potentially erosive or accretive factors<sup>8</sup>, there is a clear cause and effect relation between  
61 increasing sea levels and shoreline retreat<sup>18</sup>, pointing to increased coastal erosion issues<sup>9,19</sup>. Climate  
62 change will also affect waves and storm surges<sup>20,21</sup>, which are important drivers of coastal  
63 morphology<sup>4,5,22</sup>, and therefore considering the dynamics of extreme weather patterns is also important  
64 in assessing potential climate change impacts beyond that of SLR alone.

65 Here we present a comprehensive global analysis of sandy shoreline dynamics during the 21<sup>st</sup> century.  
66 Our probabilistic projections explicitly take into account estimates of future SLR, spatial variations of  
67 coastal morphology, ambient shoreline change trends, and future changes in meteorological drivers (e.g.  
68 storm surge and waves). We first evaluate long term shoreline change  $dx_{shore\_LT}$ , which is the result of  
69 two components: the ambient shoreline change (*AC*) driven by geological, anthropogenic and other  
70 physical factors<sup>7</sup> and the shoreline retreat due to SLR (*R*) (Supplementary Fig. S1). We obtained *AC* by  
71 extrapolating observed historical trends<sup>7</sup> within a probabilistic framework (see Methods). We computed  
72 *R* by using a modified Bruun rule<sup>18</sup> together with a new global dataset of active beach slopes<sup>23</sup>. In  
73 addition to the long term shoreline dynamics we also project how maximum erosion from coastal  
74 storms may change in view of climate change. Shoreline change projections are discussed for the years  
75 2050 and 2100 under RCP 4.5 and 8.5, relative to the baseline year 2010.

76 Our analysis shows an overall erosive trend of sandy beaches that increases in time and with the  
77 intensity of greenhouse gas emissions (Figure 1). Assuming that there are no physical limits in potential  
78 retreat, by mid-century we project a very likely (5-95<sup>th</sup> percentile) global average long term shoreline  
79 change  $dx_{shore,LT}$  ranging from -2.2 to -79.2 m and -0.8 to -99.2 m,, under RCP4.5 and RCP8.5, respectively  
80 (negative values express erosion; Supplementary Table S1). By the end of the century the erosive trend  
81 becomes even more dominant and we project a very likely range from -21.7 to -171.1 m and -42.2 to -  
82 246.9 m under RCP4.5 and RCP8.5, respectively (Figure 2 Supplementary Table S1). Moderate  
83 greenhouse gas emission mitigation could thus prevent 22% of the projected shoreline retreat by 2050  
84 and 40% by the end of the century (Supplementary Table S1). This corresponds to a global average of  
85 around 42 m of preserved sandy beach width by the end of the century.

86 The global erosive trend masks high spatial variability, with erosive and accretive tendencies  
87 interchanging across regions and along nearby coastal segments (Figure 1). Whereas local trends can  
88 exceed several meters per year, eight IPCC sub-regions show median retreats exceeding 100 m under

89 both RCPs by the end of the century (Supplementary Table S1; see Figure 2 for a definition of the  
90 regions): East North America, Amazon, Southeastern South America, Central Europe, South and West  
91 Asia, North Australia, and the Caribbean SIDS. By 2100,  $dx_{shore,LT}$  exceeds 150 m under RCP8.5 in all the  
92 above regions, while under the same scenario median retreats larger than 300 m are projected for  
93 South Asia and the Caribbean SIDS. Long term accretion is projected along sandy coastlines of East Asia  
94 under both RCPs by 2050 and only under RCP4.5 by the end of the century.

95 SLR driven retreat  $R$  is responsible for 71% and 75% of the global median shoreline change in 2050 under  
96 RCP4.5 and RCP8.5, respectively (Extended data Figs 5-6); and for 86% and 77% by the end of the  
97 century (Figure 2 and Extended Data Fig. 7). Ambient shoreline changes dominate only in certain  
98 regions, in particular in South and West Asia, West Indian Ocean, Southeastern South America, and the  
99 Caribbean SIDS regions. The contributions of the SLR retreat and ambient change to the overall  
100 uncertainty under RCP4.5 and by mid-century are relatively balanced (Extended Data Fig. 5), while AC  
101 contributes to 41% more uncertainty globally, by the end of the century (Extended Data Fig. 7). Under  
102 RCP8.5 uncertainty related to SLR retreat dominates that of AC, by 44% and 30%, by the years 2050 and  
103 2100, respectively (Extended Data Fig. 7 and Figure 2). Regionally, ambient change uncertainty is higher  
104 in North Australia South Asia.

105 The above estimates do not include the episodic, storm-driven shoreline retreat  $S$ , presently projected  
106 using the convolution erosion model of Kriebel and Dean<sup>24</sup> (see Methods). Here we discuss the 100-year  
107 event  $S$  which for the year 2050 is equivalent to circa 23% of the global average projected long term  
108 shoreline change  $dx_{shore,LT}$  (Supplementary Tables S1-4). By the end of the 21<sup>st</sup> century, the relative  
109 importance of the 100-year  $S$  compared to  $dx_{shore,LT}$  decreases to 9% and 7% under RCP4.5 and 8.5,  
110 respectively, as long term changes gather pace. Storm erosion is typically followed by beach recovery<sup>25</sup>,  
111 but some events may leave a footprint that takes decades to recover, if at all<sup>4,26</sup>, while the additional  
112 shoreline retreat renders the backshore more vulnerable to episodic coastal flooding and its  
113 consequences. Despite previous studies projecting changes in wave intensity and direction  
114 worldwide<sup>21,27,28</sup>, our projections show that overall climate change will not have a strong effect on  
115 episodic storm driven erosion. As a result, ambient and SLR driven change appear to shadow the effect  
116 of changes in storm-driven erosion, even though at certain locations  $\Delta S$  values can reach  $\pm 20$  m by the  
117 end of the century; e.g. increase in 100-year erosion potential along the South East UK, West coast of  
118 Germany, North Queensland (Australia), and Acapulco (Mexico) (Extended Data Fig. 4).

119 The projected shoreline changes will substantially impact on the shape of the world's coastline. Many  
120 coastal systems have lost already their natural capacity to accommodate or recover from erosion, as the  
121 backshore is heavily occupied by human settlements<sup>29</sup>, while dams and human development have  
122 depleted terrestrial sediment supply which would naturally replenish the shore with new material<sup>30,31</sup>.  
123 Most of the remaining regions with an extensive presence of a natural coastline, are found in Africa and  
124 Asia, which are also the regions projected to experience the highest coastal population and urbanization  
125 growth in the decades to come<sup>12,13</sup>. There is yet no global dataset on sandy beach width allowing to  
126 accurately estimate the potential loss of sandy beaches around the world. Therefore, to quantify the  
127 potential impact of our projections, we consider beaches that are projected to experience a shoreline  
128 retreat >100 m as seriously threatened by coastal erosion. The chosen 100 m threshold is rather  
129 conservative, since most sandy beaches have widths below 50 m, especially near human settlements,  
130 small islands and micro-tidal areas (e.g. Caribbean, Mediterranean).

131 We find that 10.6%-12.2% (28,260-32,456 km) of the world's sandy beaches could face severe erosion  
132 by 2050 and 37.2%-50.9% (99,996-135,279 km) by the end of the century (Extended Data Fig. 8). Thirty  
133 one percent (31%) of the world's sandy beaches are in low elevation coastal zones (LECZ) with  
134 population density exceeding 500 people per km<sup>2</sup>, and our projections show that approximately one  
135 third of these LECZ sandy coasts will be seriously threatened by erosion by the year 2050. This estimate  
136 reaches 51% and 62% by the end of the century, under RCP4.5 and RCP8.5, respectively.

137 Several countries could face extensive erosion by the end of the 21<sup>st</sup> century (along >80% of their sandy  
138 coastline under both RCPs; Figure 3) including Democratic Republic of the Congo, Gambia, Jersey,  
139 Suriname, Comoros, Palau, Benin, Guinea-Bissau, Mayotte, Iraq, Pakistan, Guinea and El Salvador. Apart  
140 from the consequent higher vulnerability to coastal hazards, several of these countries are likely to  
141 experience substantial socioeconomic implications as their economies are fragile and, tourism-  
142 dependent with sandy coastlines constituting their major tourist attraction. When the total length of  
143 sandy beaches projected to be lost by 2100 is considered (as opposed to the %), Australia emerges as the  
144 potentially most affected country, with at least 12,324 km of sandy beach coastline threatened by  
145 erosion (15,439 under RCP8.5; Extended Data Fig. 9), circa 40% of the country's total sandy coastline. By  
146 the same impact metric, Canada ranks second (9,577 and 16,651 km 15,439 under RCP4.5 and RCP8.5,  
147 respectively), followed by Chile (5,471 and 7,050 km), Mexico (4,119 and 5,105 km) China (4,084 and  
148 5,185 km), USA (3,908 and 5,553 km), Argentina (3,668 and 4,413 km) and Iran (3,654 and 3,870 km).

149 Past experience has shown that effective site-specific coastal planning can mitigate beach erosion,  
150 eventually resulting in a stable coastline; with the most prominent example being the Dutch coast<sup>32</sup>. A  
151 positive message from the present analysis is that while SLR will drive shoreline retreat almost  
152 everywhere, many locations show ambient erosive trends related to human interventions<sup>7</sup>, which in  
153 theory could be avoided by more sustainable coastal zone and catchment management practices. At the  
154 same time, the range of projected SLR implies unprecedented pressure to our coasts which requires the  
155 development and implementation of informed and effective adaptive measures.

## 156 CORRESPONDENCE

157 Correspondence and requests for materials should be addressed to M.I.V.

## 158 References

- 159 1 Luijendijk, A. *et al.* The State of the World's Beaches. *Scientific Reports* **8**, 6641,  
160 doi:10.1038/s41598-018-24630-6 (2018).
- 161 2 Barbier, E. B. *et al.* The value of estuarine and coastal ecosystem services. *Ecological*  
162 *Monographs* **81**, 169-193, doi:10.1890/10-1510.1 (2011).
- 163 3 Temmerman, S. *et al.* Ecosystem-based coastal defence in the face of global change. *Nature* **504**,  
164 79, doi:10.1038/nature12859 (2013).
- 165 4 Masselink, G. *et al.* Extreme wave activity during 2013/2014 winter and morphological impacts  
166 along the Atlantic coast of Europe. *Geophys. Res. Lett.* **43**, 2135-2143,  
167 doi:10.1002/2015GL067492 (2016).
- 168 5 Barnard, P. L. *et al.* Coastal vulnerability across the Pacific dominated by El Nino/Southern  
169 Oscillation. *Nat. Geosci.* **8**, 801-807, doi:10.1038/ngeo2539 (2015).
- 170 6 Cooper, J. A. G., Green, A. N. & Loureiro, C. Geological constraints on mesoscale coastal barrier  
171 behaviour. *Global Planet. Change* **168**, 15-34,  
172 doi:https://doi.org/10.1016/j.gloplacha.2018.06.006 (2018).
- 173 7 Mentaschi, L., Vousdoukas, M. I., Pekel, J.-F., Voukouvalas, E. & Feyen, L. Global long-term  
174 observations of coastal erosion and accretion. *Scientific Reports* **8**, 12876, doi:10.1038/s41598-  
175 018-30904-w (2018).
- 176 8 Ranasinghe, R. Assessing climate change impacts on open sandy coasts: A review. *Earth-Science*  
177 *Reviews* **160**, 320-332, doi:https://doi.org/10.1016/j.earscirev.2016.07.011 (2016).
- 178 9 Hinkel, J. *et al.* A global analysis of erosion of sandy beaches and sea-level rise: An application of  
179 DIVA. *Global Planet. Change* **111**, 150-158, doi:https://doi.org/10.1016/j.gloplacha.2013.09.002  
180 (2013).
- 181 10 Koks, E. E. *et al.* A global multi-hazard risk analysis of road and railway infrastructure assets.  
182 *Nature Communications* **10**, 2677, doi:10.1038/s41467-019-10442-3 (2019).
- 183 11 McGranahan, G., Balk, D. & Anderson, B. The rising tide: assessing the risks of climate change  
184 and human settlements in low elevation coastal zones. *Environment and Urbanization* **19**, 17-37,  
185 doi:10.1177/0956247807076960 (2007).
- 186 12 Neumann, B., Vafeidis, A. T., Zimmermann, J. & Nicholls, R. J. Future Coastal Population Growth  
187 and Exposure to Sea-Level Rise and Coastal Flooding - A Global Assessment. *PLOS ONE* **10**,  
188 e0118571, doi:10.1371/journal.pone.0118571 (2015).

189 13 Jones, B. & O'Neill, B. C. Spatially explicit global population scenarios consistent with the Shared  
190 Socioeconomic Pathways. *Environmental Research Letters* **11**, doi:10.1088/1748-  
191 9326/11/8/084003 (2016).

192 14 Davenport, J. & Davenport, J. L. The impact of tourism and personal leisure transport on coastal  
193 environments: A review. *Estuar. Coast. Shelf Sci.* **67**, 280-292,  
194 doi:https://doi.org/10.1016/j.ecss.2005.11.026 (2006).

195 15 Nerem, R. S. *et al.* Climate-change-driven accelerated sea-level rise detected in the altimeter  
196 era. *Proceedings of the National Academy of Sciences* **115**, 2022-2025,  
197 doi:10.1073/pnas.1717312115 (2018).

198 16 Bamber, J. L., Oppenheimer, M., Kopp, R. E., Aspinall, W. P. & Cooke, R. M. Ice sheet  
199 contributions to future sea-level rise from structured expert judgment. *Proceedings of the*  
200 *National Academy of Sciences*, 201817205, doi:10.1073/pnas.1817205116 (2019).

201 17 Jevrejeva, S., Jackson, L. P., Riva, R. E. M., Grinsted, A. & Moore, J. C. Coastal sea level rise with  
202 warming above 2 °C. *Proceedings of the National Academy of Sciences* **113**, 13342-13347,  
203 doi:10.1073/pnas.1605312113 (2016).

204 18 Bruun, P. Sea level rise as a cause of shore erosion. *Journal of Waterway, Harbors Division. ASCE*  
205 **88**, 117 (1962).

206 19 Anthony, E. J. *et al.* Linking rapid erosion of the Mekong River delta to human activities.  
207 *Scientific Reports* **5**, 14745, doi:10.1038/srep14745 (2015).

208 20 Vousdoukas, M. I. *et al.* Global probabilistic projections of extreme sea levels show  
209 intensification of coastal flood hazard. *Nature Communications* **9**, 2360, doi:10.1038/s41467-  
210 018-04692-w (2018).

211 21 Hemer, M. A., Fan, Y., Mori, N., Semedo, A. & Wang, X. L. Projected changes in wave climate  
212 from a multi-model ensemble. *Nature Clim. Change* **3**, 471-476, doi:10.1038/nclimate1791  
213 (2013).

214 22 Slott, J. M., Murray, A. B., Ashton, A. D. & Crowley, T. J. Coastline responses to changing storm  
215 patterns. *Geophys. Res. Lett.* **33**, doi:10.1029/2006GL027445 (2006).

216 23 Athanasiou, P. *et al.* A global dataset of coastalslopes for coastal recession assessments. *Earth*  
217 *System Science Data Discussions* **11**, 1515–1529, doi:https://doi.org/10.5194/essd-11-1515-  
218 2019 (2019).

219 24 Kriebel, D. L. & Dean, R. G. Convolution method for time dependent beach profile response.  
220 *Journal of Waterway, Port, Coastal and Ocean Engineering* **119**, 204-226 (1993).

221 25 Vousdoukas, M. I. Erosion/accretion patterns and multiple beach cusp systems on a meso-tidal,  
222 steeply-sloping beach. *Geomorphology* **141**, 34-46, doi:10.1016/j.geomorph.2011.12.003 (2012).

223 26 Anderson, T. R., Frazer, L. N. & Fletcher, C. H. Transient and persistent shoreline change from a  
224 storm. *Geophys. Res. Lett.* **37**, doi:10.1029/2009gl042252 (2010).

225 27 Erikson, L. H., Hegermiller, C. A., Barnard, P. L., Ruggiero, P. & van Ormondt, M. Projected wave  
226 conditions in the Eastern North Pacific under the influence of two CMIP5 climate scenarios.  
227 *Ocean Modelling* **96**, 171-185, doi:https://doi.org/10.1016/j.ocemod.2015.07.004 (2015).

228 28 Mentaschi, L., Vousdoukas, M. I., Voukouvalas, E., Dosio, A. & Feyen, L. Global changes of  
229 extreme coastal wave energy fluxes triggered by intensified teleconnection patterns. *Geophys.*  
230 *Res. Lett.* **44**, 2416-2426, doi:10.1002/2016GL072488 (2017).

231 29 Small, C. & Nicholls, R. J. A Global Analysis of Human Settlement in Coastal Zones. *J. Coast. Res.*  
232 **19**, 584-599 (2003).

233 30 Milliman, J. D. Blessed dams or damned dams? *Nature* **386**, 325-327, doi:10.1038/386325a0  
234 (1997).

235 31 Ranasinghe, R., Wu, C. S., Conallin, J., Duong, T. M. & Anthony, E. J. Disentangling the relative  
236 impacts of climate change and human activities on fluvial sediment supply to the coast by the  
237 world's large rivers: Pearl River Basin, China. . *Scientific Reports* (accepted).

238 32 Brière, C., Janssen, S. K. H., Oost, A. P., Taal, M. & Tonnon, P. K. Usability of the climate-resilient  
239 nature-based sand motor pilot, The Netherlands. *J. Coast. Conserv.* **22**, 491-502,  
240 doi:10.1007/s11852-017-0527-3 (2018).

241

## 242 Figure captions

243 *Figure 1. Projected long term shoreline change. By the year 2050 (a,c) and 2100 (b,d) under RCP4.5 (a-b) and RCP8.5 (c-d).*  
244 *Values represent the median change and positive/negative values respectively express accretion/erosion in m, relative to 2010.*  
245 *The global average median change is shown in the inset text for each case, along with the 5th-95th percentile range.*

246

247 *Figure 2. Projected median long term shoreline change under RCP8.5 by the year 2100 ( $dx_{shore,LT}$ ), for the 26 IPCC SREX sub-*  
248 *regions and the worldwide average. For the horizontal bar plot on right; positive/negative values express accretion/erosion in m;*  
249 *black error bars indicate the 5<sup>th</sup>-95<sup>th</sup> quantile range. Shoreline change is considered to be the result of SLR retreat (R) and*  
250 *ambient shoreline change trends (AC). Pie plots show the relative contributions of R and AC to the projected median  $dx_{shore,LT}$ ,*  
251 *with transparent slices expressing accretive trends. Vertical bar plots show the ratio between the uncertainty of R and AC (5<sup>th</sup>-*  
252 *95<sup>th</sup> quantile range), to the total uncertainty in projected median  $dx_{shore,LT}$ .*

253

254 *Figure 3. Per country percentages of the sandy coastline length which is projected to retreat by more than 100 m. By 2050 (a,c)*  
255 *and 2100 (b,d), under RCP4.5 (a-b) and RCP8.5 (c-d). Values are based on the median long term shoreline change, relative to*  
256 *2010.*

257



# 258 1 Methods

## 259 1.1 General concepts

260 In this study we project shoreline dynamics throughout this century along the world's sandy coastlines  
261 under two Representative Concentration Pathways (RCPs): RCP4.5 and RCP8.5. RCP4.5 may be viewed  
262 as a *moderate-emission-mitigation-policy scenario* and RCP8.5 as a *high-emissions scenario*<sup>33</sup>. The study  
263 focusses on the evolution of three components of sandy beach shoreline dynamics (Supplementary Fig.  
264 S1):

- 265 - *AC*: Ambient shoreline dynamics driven by long-term hydrodynamic, geological and anthropic  
266 factors.
- 267 - *R*: Shoreline retreat due to coastal morphological adjustments to Sea Level Rise (SLR).
- 268 - *S*: Episodic erosion during extreme storms.

269 The first two components represent longer term shoreline changes and are quantified here as:

$$270 \quad dx_{shore,LT} = AC + R \quad 1$$

271 *AC* expresses long-term ambient shoreline dynamics that can be driven by a wide range of natural  
272 and/or anthropogenic processes, excluding the effect of SLR (*R*) and that of episodic erosion during  
273 extreme events (*S*; see following paragraph). In most cases *AC* is related to human interventions that  
274 alter the sediment budget and/or transport processes of coastal systems<sup>7</sup>, but it also includes natural  
275 transitions due to a variety of reasons, such as weather patterns<sup>4,34-36</sup>, persistent longshore transport  
276 variations<sup>37</sup>, or geological control<sup>38,39</sup>. *R* in Eq. 1 represents SLR-driven shoreline retreat, the magnitude  
277 of which depends on the transfer of sediment from the sub-aerial to the submerged part of the active  
278 beach profile, in order to adjust to rising Mean Sea Levels (MSLs).

279 The third component *S* represents episodic erosion from intense waves and storm surges during  
280 extreme weather events. Episodic erosion is usually followed by a recovery process<sup>40-42</sup>. It is assumed  
281 here that the irreversible net effect of episodic erosion and post-storm recovery constitutes part of the  
282 ambient shoreline evolution expressed by *AC*. *S* is therefore limited to the reversible episodic shoreline  
283 retreat during storm events relative to its long term position expressed by  $dx_{shore,LT}$ . Potential variations  
284 in storminess with global warming will induce changes in *S* compared to present day conditions.

285 At any point in time, the maximum shoreline retreat  $dx_{shore,max}$  during an extreme coastal event due to  
286 the combined effects of long-term and episodic erosion is then defined as

$$287 \quad dx_{shore,max} = AC + R + S \quad 2$$

288 Each of these components are discussed in more detail below.

289 This study focuses on ice-free sandy beaches, which constitute the most common and dynamic beach  
290 type globally, covering more than 30% of the ice-free coastline in the world<sup>1,43</sup>. While in reality shoreline  
291 retreat can be limited by the presence of natural or anthropogenic barriers, spatial data on such  
292 features is not available globally at the resolution needed for the present study. Adaptive measures  
293 against beach erosion could have a similar effect, but are difficult to predict and merit a separate study.  
294 Therefore, we do not invoke any physical limits to the extent of potential shoreline retreat.

## 295 1.2 Ambient shoreline dynamics

296 Several parts of the global coastline undergo long-term ambient changes as a result of various  
297 hydrodynamic, geological and anthropic factors. Historical shoreline trends were estimated by  
298 Mentaschi et al.<sup>7</sup> from the high-resolution Global Surface Water (GSW) database<sup>44</sup>. It provides spatio-  
299 temporal dynamics of surface water presence globally at 30 m resolution from 1984 to 2015, obtained  
300 by the automated analysis of over 3 million Landsat satellite images. This GSW dataset was processed  
301 for changes in water presence in coastal areas to produce time series of cross-shore shoreline position<sup>7</sup>.  
302 The pixel-wise information of GSW was translated into cross-shore shoreline dynamics using a set of  
303 over 2,000,000 shore-normal transects. The transects were defined every 250 m along a global coastline  
304 obtained from OpenStreetMap<sup>45</sup> and were sufficiently long to accommodate the shoreline displacement  
305 during the study period. Each transect defines a 200 m alongshore-wide coastal section, along which  
306 surface water transitions were considered in order to extract time-series of shoreline displacement  
307 along each shore normal transect.

308 We consider as a proxy for the shoreline change the cross-shore displacement of the seaward boundary  
309 of the ‘permanent land layer’; i.e. the areas where water presence has never been detected throughout  
310 the year. Over the 32-year period considered, the selected proxy can respond to tidal, storm surge,  
311 wave and swash dynamics, as well as the inter-related dynamics of the beach face slope or nearshore  
312 bathymetry. Among the different shoreline definitions proposed in literature<sup>46</sup>, the present one was  
313 chosen as it is more compatible with the type of analysis and the spatial and temporal resolution of the

314 satellite dataset<sup>46</sup>. A detailed description of the procedure, the data, and also links to the final dataset  
315 can be found in Pekel et al.<sup>44</sup>, and Mentaschi et al.<sup>7</sup>.

316 For the purpose of determining AC in the present study, we consider shoreline dynamics data for a 32-  
317 year period (1984-2015) from Mentaschi et al.<sup>7</sup>. We assume that this time series is representative for  
318 present-day ambient shoreline changes and extrapolate the trend into the future using a probabilistic  
319 approach. For each location, we consider the time series of all transects that are within 5 km distance  
320 along the same coastline stretch. This acts as a spatial smoothing in order to filter out local trends and  
321 reflects changes at km scale, which are more relevant in a global scale analysis. It further ensures that  
322 each transect has sufficient data and compensates for gaps in the satellite measurements due to poor  
323 quality or lack of data. The original dataset comes with confidence indicators and low-confidence  
324 measurements are excluded from the analysis. Similarly, shoreline changes that exceed 5 km in a year  
325 are also excluded as outliers.

326 The above analysis results in sets of annual shoreline displacements for each point, which are sampled  
327 randomly to generate synthetic series of future shoreline position with an annual time step. The Monte  
328 Carlo sampling results in one million realizations of future shoreline evolution, resulting in Probability  
329 Density Functions (PDFs) of annual shoreline displacement during the present century in each transect.  
330 The number of realizations was taken to ensure a stable PDF of the shoreline changes by the end the  
331 century in all studied transects, i.e. when the mean and the standard deviation of the PDFs converged.  
332 The realizations of future shoreline evolution assume that ambient change will follow historical trends  
333 and express the uncertainty of the historical observations.

### 334 1.3 Shoreline retreat due to SLR

335 The estimation of the equilibrium shoreline retreat  $R$  of sandy coasts due to SLR is based on the Bruun  
336 rule<sup>18</sup>. This approach builds on the concept that the beach morphology tends to adapt to the prevailing  
337 wave climate and is given by:

$$338 \quad R = \frac{1}{\tan\beta} SLR \quad 3$$

339

340 where  $\tan\beta$  is the active profile slope.

341 Projections of regional SLR up to the end of this century are available from a probabilistic, process-based  
342 approach<sup>47</sup> that combines the major factors contributing to SLR: impact of self-attraction and loading of

343 the ocean upon itself due to the long term alteration of ocean density changes, globally averaged steric  
344 sea-level change, dynamic sea-level change, surface mass balance of ice from glaciers and ice-caps,  
345 surface mass balance and ice dynamics of Greenland and Antarctic ice sheet, land-water storage and  
346 Glacial Isostatic Adjustment. Local smaller scale vertical land movements such as land subsidence due to  
347 for example ground water pumping are not included in the SLR projections.

348 The  $\tan\beta$  term in equation 3 expresses the slope of the active beach profile, which to date typically has  
349 been assumed to be constant (in space) in large scale studies<sup>9</sup>. Here, we use a newly released global  
350 dataset of active beach slopes<sup>23</sup>. The dataset has been created combining the MERIT digital elevation  
351 dataset<sup>48</sup> with the GEBCO bathymetry<sup>49</sup>. Beach profiles are generated along each sandy beach transect  
352 by combining the above bathymetric and topographic data. The offshore boundary of the active profile  
353 is defined by the furthest location from the coast with a depth equal to the depth of closure  $d_c$ . The  
354 latter is calculated using an adaptation of the original Hallermeier 1978<sup>50</sup> formula by Nicholls et al. 1998<sup>51</sup>  
355 for applications on longer time scales, given by:

$$356 \quad d_c = 2.28H_{e,t} - 68.5 \left( \frac{H_{e,t}^2}{gT_{e,t}^2} \right) \quad 4$$

357 where  $H_{e,t}$  is the significant wave height that is exceeded only 12 hours per  $t$  years,  $T_{e,t}$  is the associated  
358 wave period, and  $g$  is the gravitational acceleration. In this case  $t$  is equivalent to the 1980-2100 period.

359 The landward active profile boundary varies among studies and has been defined as the crest of the  
360 berm or dune, or the most offshore location with an elevation equal to the MSL. In the absence of  
361 reliable estimates of the dune or berm height  $B$ , and following the original definition of the Bruun Rule<sup>18</sup>  
362 and its application in several recent studies<sup>9,52,53</sup>, here we take the MSL contour as the landward active  
363 profile boundary. The cross-shore distance between these two points is considered as the length of the  
364 active profile  $L_b$ , of which the slope is defined as  $\tan\beta = \frac{d_c}{L_b}$ .

365 Waves are simulated over the period 1980 to 2100 using the third generation spectral wave model  
366 WAVEWATCH-III forced by atmospheric conditions from 6 CMIP5 GCMs<sup>28,54</sup>. The model runs on a global  
367  $1.5^\circ$  grid, combined with several nested finer sub-grids with resolution varying from  $0.5^\circ$  to  $0.5^\circ$ . The  
368 model's skill to reproduce global wave fields was assessed by comparing time series from a reanalysis  
369 covering 35 years between 1980 and 2014, forced by ERA-Interim wind data, against altimeter data  
370 provided by 6 different satellites<sup>55</sup>: ERS-2, ENVISAT, Jason 1 and 2, Cryosat 2 and SARAL-AltiKa. Point  
371 measurements provided by buoys were used for additional validation. Detailed information on the  
372 model set-up and validation can be found in the references provided<sup>28,54</sup>.

373 Several recent studies in Australia<sup>41</sup>, Netherlands<sup>56</sup>, Spain<sup>57</sup> and France<sup>58</sup> that compared coastline retreat  
374 projections obtained via the physics based Probabilistic coastline recession (PCR) model with those  
375 derived with the Bruun rule have indicated that the latter consistently provides higher-end estimates of  
376 coastline retreat. Acknowledging that the extent of overestimation depends on site-specific factors, we  
377 therefore include in our probabilistic framework a correction factor  $E$ , which varies randomly between  
378 0.1 and 1.0 centered around a conservative median value 0.75. Thus, here we compute SLR driven  
379 shoreline retreat using the equation:

$$380 \quad R = E \cdot \frac{1}{\tan\beta} \cdot SLR \quad 5$$

381 Finally, the active beach slope analysis detected that  $\tan\beta$  values in some parts of the world can be as  
382 mild as 1/800. According to the Bruun rule and the projected range of SLR, such mild sloping coastal  
383 zones will experience shoreline retreats of several hundreds of meters. While not impossible, such  
384 estimates could yield serious potential overestimations of real-world shoreline adjustment to SLR<sup>59</sup>. We  
385 therefore limit the minimum beach slope to 1/300, which is a realistic lower bound estimate for sandy  
386 beaches.

387 As SLR retreat is estimated in a probabilistic manner through Monte Carlo simulations, the resulting  
388 PDFs express the uncertainty from the SLR projections and the Bruun rule error expressed through the  $E$   
389 correction factor.

#### 390 1.4 Storm-induced erosion

391 Episodic erosion during extreme storms is estimated using the convolution erosion model KD93 of  
392 Kriebel and Dean<sup>24</sup>. KD93 is based on the equilibrium profile concept and estimates shoreline retreat  
393 and volumetric sand loss due to extreme waves and storm surge. KD93 input can be classified in (i)  
394 hydrodynamic variables: significant wave height ( $H_s$ ), peak wave period ( $T_p$ ), wave incidence angle ( $\alpha_w$ ),  
395 storm surge ( $\eta_s$ ), tidal level ( $\eta_{tide}$ ) and event duration; and (ii) parameters related to the beach profile:  
396 dune height  $D$ , berm height  $B$  and width  $W$ , and the beach-face slope  $\tan\beta_f$ .

397 Storm surges for the present and future climate conditions are simulated using the DFLOW FM  
398 model<sup>60,61</sup> forced with the same 6-member CMIP5 Global Climate Model (GCM) ensemble as the wave  
399 projections<sup>20</sup> (described in the previous section).

400 The hydrodynamic conditions driving episodic beach erosion are obtained from the wave and storm  
401 surge projections. For each of the 6 GCMs we extracted the storm events simulated during the period

402 1980-2100, considering the parameters:  $\max H_s$ ,  $\eta_s$ ,  $\eta_{tide}$  and  $T_p$ , as well as mean wave direction  $Dir_w$ , and  
403 event duration. The extraction of storm events is based on the following criteria: (i) maximum  $H_s$  or  $\eta_s$   
404 exceeding the 90<sup>th</sup> percentile value; (ii) maximum  $T_p$  above 3 s; and (iii) maximum  $H_s$  above 0.5 m.

405 The offshore wave conditions are transformed to the nearshore (50 m depth) through wave refraction,  
406 shoaling and breaking calculations based on Snell's law, following the approach described in Part II,  
407 Chapter 2 of the US Army Corps Coastal engineering Manual<sup>62</sup>. The wave incidence angle required for  
408 the calculations is obtained by combining the wave direction of each event from the model output with  
409 the mean shoreline orientation. The active beach slope is obtained from the global dataset mentioned  
410 above<sup>23</sup>.

411 Subsequently, we simulate storm induced erosion for all the above events using KD93 on equilibrium  
412 profiles, obtaining a sequence of shoreline retreat events for each transect. Subsequently, we apply  
413 non-stationary extreme value statistical analysis<sup>63</sup> and fit a generalized Pareto distribution to the retreat  
414 event series in order to obtain shoreline retreat estimates for different return periods. The present  
415 analysis focuses on the storm-induced shoreline retreat for the 100-year retreat event  $S_{100}$ , and its  
416 difference ( $\Delta S_{100}$ ) compared to present day conditions.

417 As storm retreat is estimated in a probabilistic manner through Monte Carlo simulations, the resulting  
418 PDFs express the uncertainty from the wave projections (i.e. GCM ensemble spread and ocean model  
419 error).

## 420 1.5 Spatial analysis

421 The study focusses on sandy beaches along the global coastline, which have been detected in a recent  
422 study by discretizing the coast at 500 m alongshore transects<sup>1</sup>. We use the Global Human Settlement  
423 Layer<sup>64</sup> to estimate the population in low-lying coastal areas (i.e. elevation <10 m MSL) within a distance  
424 of 25 km from each sandy beach transect. This serves as a proxy for the number of people benefiting  
425 from nearby sandy beaches; either receiving natural protection from coastal storms, or benefiting from  
426 beach amenity value, or other socio-economic activities related to tourism, beach-use, etc.

427 In order to identify regional patterns in shoreline dynamics, the global coastline is divided in 26  
428 geographical regions (Extended Data Fig. 1), as defined in the IPCC Special Report on Managing the Risks  
429 of Extreme Events and Disasters to Advance Climate Change Adaptation<sup>65</sup>. The values discussed in the  
430 manuscript correspond to averages for each region and country, or for the entire global coastline.

## 431 1.6 Statistical analysis

432 Equations 1 and 2 are applied here in a probabilistic manner, with the assumption that shoreline change  
433 components  $R$ ,  $S$  and  $AC$  are independent. PDFs of the three components are combined through Monte  
434 Carlo simulations following the steps below<sup>20</sup>: (i) random sampling from the individual PDFs; (ii) linear  
435 addition of the  $dx_{shore}$  components according to equations 1 and 2; (iii) control of convergence to ensure  
436 that the number of realizations is sufficient; (iv) joint PDF estimation. Typically one million realizations  
437 are sufficient to obtain stable PDFs and convergence of the final percentiles. The resulting PDF of  $dx_{shore}$   
438 expresses the joint contributions from all components and the uncertainty therein (uncertainty factors  
439 considered for each component are discussed in the final paragraph of the different dedicated sections  
440 1.2-1.4).

441 We express the relative contribution of a component by the fraction of its median value to the median  
442 total retreat. Similarly, relative contributions to the total  $dx_{shore}$  uncertainty is expressed by the fraction  
443 of each component's variance to the total variance. We also estimate the difference between the  
444 median  $dx_{shore}$  values for RCP4.5 and RCP8.5.

## 445 1.7 Limitations

446 The spatial and temporal scale of the analysis presented here imposes inevitable limitations related to  
447 computational resources, data availability and methodological abstraction, the most important of which  
448 are discussed below.

449 Ambient shoreline trends can be an important component of shoreline dynamics and depend on several  
450 factors including the various sediment sources and sinks<sup>57</sup>, along with the fate of sediments<sup>66-68</sup>. While  
451 smaller-scale assessments considered in detail the above factors<sup>69</sup>, limitations in terms of modelling  
452 capabilities and available datasets, render application of such a methodology at global scale as  
453 impossible. Therefore, in the present analysis we extrapolate historically observed ambient shoreline  
454 changes  $AC$  into the future, as is common in previous studies<sup>58,70,71</sup>. This is done, however, in a  
455 probabilistic way that allows quantifying the temporal variability and inherent uncertainty. As such,  
456 future ambient shoreline dynamics follow ongoing trends within uncertainty bounds defined by the  
457 spread of the observed historical changes. The 32 year time window considered may be long enough to  
458 express decadal-scale variability in shoreline position, but still may not fully resolve some rare cases of  
459 coastline change, like those induced by very extreme events, or sudden and drastic human

460 interventions. Finally, the 30 m spatial resolution of the satellite dataset may not suffice to resolve  
461 smaller displacements in less energetic areas.

462 Shoreline retreat due to SLR is estimated using the Bruun rule<sup>18</sup>, which despite its known drawbacks is  
463 expected to be adequate for large scale assessments<sup>9,72</sup>. The Bruun rule is based on the concept that the  
464 morphology tends to reach an equilibrium state, which is supported by field observations<sup>40,73,74</sup>.  
465 However, the parameterization of the equilibrium profile *per se* has been a subject of debate<sup>75-77</sup>, as the  
466 simplified model excludes several factors controlling coastal morphology often found in nature. These  
467 include, for example, sediment sinks and sources<sup>69</sup>, morphological response to SLR<sup>59</sup>, morphological  
468 control from natural or artificial structures<sup>6</sup>, the presence of nearshore bars<sup>78</sup> or other morphological  
469 features<sup>79,80</sup> and longshore processes<sup>66</sup>.

470 Still, despite the criticism<sup>75</sup>, the concept is being used extensively because any proposed improvements  
471 and modifications<sup>53,81-85</sup> demand data that are often not available. In the present implementation  
472 several of the shortcomings of the Bruun rule are bypassed since  $R$  focusses only on what the concept  
473 can deliver; i.e. alongshore-averaged shoreline response to SLR and changes in wave climate. Most of  
474 the factors discussed above and that are beyond the Bruun rule's capacity are expressed by the ambient  
475 change AC: e.g. changes due to sediment budget imbalances, geological or anthropogenic factors.

476 The uncertainty related to the active profile slope is another common weakness of the Bruun rule<sup>41</sup>,  
477 which in the present analysis is addressed through the use of estimates obtained from topo-bathymetric  
478 data. The quantitative accuracy of Bruun rule estimates has also been the subject of rigorous debate for  
479 over 3 decades<sup>41,72,75,86</sup>. Here we have attempted to address this source of uncertainty by incorporating a  
480 correction factor  $E$  (Eq 5; see also discussion in Section 1.3), which is implemented probabilistically  
481 within the Monte Carlo framework adopted in our computations.

482 Beach profile responses to storms are simulated using the KD93 model, rather than with sophisticated  
483 process-based models that incorporate elaborate numerical methods and sediment transport  
484 modules<sup>87-93</sup>. Such models can potentially provide more accurate estimations of storm erosion (if they  
485 are well calibrated and validated), but require as input detailed topo-bathymetric and sediment grain  
486 size information that is not available at global scale. The present analysis of  $S$  required the simulation of  
487 circa 45 million storm events, rendering the application of models that are computationally more  
488 expensive than KD93 practically impossible. In addition, KD93 has produced acceptable results in  
489 previous smaller-scale applications of similar scope<sup>94-96</sup>.



490 An aspect not covered in our analysis is the effect of storm clusters. It has been discussed extensively in  
491 previous studies, based either on field data<sup>40,42</sup>, or numerical models<sup>87,97-99</sup>, that storm chronology can  
492 enhance the impact of individual events. These studies have also shown that storm erosion can be  
493 followed by beach recovery. The latter is a complex process that is difficult to simulate<sup>73,100</sup> and requires  
494 in situ data. Predicting the maximum erosion from storm clusters at global scale is therefore a  
495 challenging task. We consider only the episodic erosion from individual storms without accounting for  
496 storm groups and do not simulate post-storm recovery. Rather it is assumed that the combined, long-  
497 term, residual effects of erosion and recovery are included in the ambient change component AC.

498 The present analysis assumes unlimited backshore space for shoreline retreat. Some natural coastal  
499 systems may have such accommodation space, while in other sites this may be strongly limited by  
500 human development or physical barriers. This is a known issue which combined with SLR can have  
501 societal and ecological implications discussed in the literature, especially under the term of coastal  
502 squeeze<sup>101,102</sup>. In principle, satellite imagery could provide information on beach width<sup>103</sup> and available  
503 space for coastal retreat at the backshore, yet such global dataset is not available. Socio-economic  
504 projections suggest that coastal development will most likely continue in the decades to come<sup>12,13</sup>,  
505 which may further reduce the accommodating space for coastal retreat. We consider arbitrary erosion  
506 threshold values to indicate potential changes that could be critical for sandy beaches. With the  
507 information on backshore space and development that may be available at local/regional scales, our  
508 publicly available projections could be used by scientists and practitioners to carry out more detailed  
509 smaller-scale assessments.

## 510 1.8 Additional Results

### 511 [Sea level rise retreat](#)

512 Rising sea levels will result in shoreline retreat along the entire global coastline with the exception of a  
513 few regions that experience uplift, like the Baltic Sea (Extended Data Fig. 2). The global average median  
514  $R$  by 2050 (relative to 2010) is projected to be around -28 m and -35 m under RCP4.5 and RCP8.5,  
515 respectively. By the end of the century, SLR-driven erosion is projected to further grow to around -63 m  
516 and -105 m, respectively. The retreat of sandy beaches due to SLR is projected to be highest (at least 130  
517 m by 2100 relative to 2010 under RCP8.5) in North Australia, Central North America, North-East Brazil,  
518 South and Southeast Asia, and Central Europe. Other regions for which high  $R$  values are projected  
519 include West Africa, Southeastern South America, South Australia/New Zealand, East Asia and East  
520 North America.

## 521 Ambient changes

522 The present section discusses long-term ambient changes as a result of hydrodynamic, geological and  
523 anthropic factors. The global averaged AC is erosive, corresponding to global average land retreat of -  
524 11.5 m by 2050 (very likely range between -34.7 and 11.7 m) and of -30.4 m by the end of the century  
525 (very likely range between -79.1 and 18.2 m). The stronger erosion is projected for South Asia, the  
526 Caribbean SIDS, and Southeastern South America with the very likely range by the end of the century  
527 being from -431.8 to -238.2, from -250 to -174.2, and from -204.5 to -71.3, respectively (Extended Data  
528 Fig. 3). East Asia shows a strong accretive ambient shoreline change trend (very likely range: 86.7-147.6),  
529 being the result of major coastal land reclamations over the recent decades.

530 Smaller scale projections show high spatial variability with erosive and accretive trends interchanging.  
531 Examples of accretion hotspots in Central America/Mexico can be found in Colombia, both on the  
532 Caribbean Sea and on the Pacific Ocean, especially at the mouths of the rivers Atrato, Sinu, Magdalena,  
533 Jurubida, San Juan and others. In Central North America, the long-term trends of coastal  
534 erosion/accretion are dominated by the dynamics at the mouth of the Mississippi river. The area is very  
535 dynamic, with large erosive spots (e.g. the Terrebonne Bay) and accretive spots (e.g. the Atchafalaya  
536 delta<sup>104</sup>). Furthermore, the area is frequently hit by tropical cyclones<sup>105</sup> that may cause abrupt extreme  
537 erosion, for example hurricane Katrina, the largest natural disaster in the history of the US<sup>106</sup>, and  
538 hurricane Rita in 2005.

539 In North-Eastern Brazil, the activity is dominated by the morpho-dynamics of the Tocantins delta and  
540 along the coasts of Para-Maranhao-Piaui-Ceara, a very active area characterized by both extreme  
541 coastal erosion and accretion<sup>7</sup>. The dominance of accretion is likely due to the erosivity of the soil in the  
542 interior, a rich river network that transports sediments towards the sea, and strong macro-tidal currents  
543 carrying them along the coasts<sup>107</sup>.

544 The most active areas in Southern Africa are the coasts of Mozambique and the Western coasts of  
545 Madagascar, areas characterized by intense tidal currents. Accretion prevails especially in Madagascar,  
546 likely due to internal erosion and subsequent transport of sediment towards the coasts, and  
547 redistribution of it by currents<sup>108</sup>.

548 Southeast Asia is characterized by both extreme erosion and accretion. Intense erosion can be observed,  
549 for example, at the deltas of the rivers Sittaung<sup>109</sup> and Mekong<sup>19</sup>, or in areas of strong land subsidence,  
550 like the Northern coast of Java<sup>110</sup>, or in the northern Manila Bay<sup>111</sup>. Examples of areas dominated by  
551 extreme accretion are the extended delta of the Red river in North Vietnam, western New Guinea,

552 several river deltas in the Malaysian peninsula and Sumatra, as well as in intensely built sites such as  
553 Bangkok and Singapore. A more detailed discussion on the local/regional variations can be found in  
554 Mentaschi et al.<sup>7</sup>.

## 555 Acknowledgments

556 RR is supported by the AXA Research fund and the Deltares Strategic Research Programme 'Coastal and  
557 Offshore Engineering'. PA is supported by the EU Horizon 2020 Programme for Research and Innovation,  
558 under grant agreement no. 776613 (EUCP: EUropean Climate Prediction system).

## 559 Author contributions

560 M.I.V, R.R. and L.F. jointly conceived the study. M.I.V. and L.M. produced the storm surge and wave  
561 projections. L.M. produced the ambient shoreline change data. M.I.V. and T.A.P. produced the storm  
562 erosion and sea level rise retreat projections, P.A. produced the global beach slope dataset, A.L.  
563 produced the global sandy beach presence dataset. M.I.V. analysed the data and prepared the  
564 manuscript, with all authors discussing results and implications and commenting on the manuscript at  
565 all stages. T.P. was funded by the research group RNM-328 of the Andalusian Research Plan (PAI) and  
566 the Portuguese Science and Technology Foundation (FCT) through the grant UID/MAR/00350/2013  
567 attributed to CIMA of the University of Algarve. The corresponding author would like to thank Drs  
568 Alessio Giardino and Ap van Dongeren for providing helpful comments on the manuscript and the  
569 methodology.

570 **Competing interests:** the Authors declare no Competing Financial or Non-Financial Interest

## 571 Data availability

572 The models and datasets presented are part of the integrated risk assessment tool LISCoAsT (Large scale  
573 Integrated Sea-level and Coastal Assessment Tool) developed by the Joint Research Centre of the  
574 European Commission. The dataset is available through the LISCoAsT repository of the JRC data  
575 collection (<http://data.europa.eu/89h/18eb5f19-b916-454f-b2f5-88881931587e>) and should be cited as  
576 follows:

577 European Commission, Joint Research Centre (2019): Global shoreline change projections.

578 European Commission, Joint Research Centre (JRC) [Dataset] doi:10.2905/18EB5F19-B916-454F-B2F5-  
579 88881931587E; PID: <http://data.europa.eu/89h/18eb5f19-b916-454f-b2f5-88881931587e>

## 580 Code availability

581 The code that supported the findings of this study is available from the corresponding author upon  
582 reasonable request.

## 583 Methods References

- 584 33 Meinshausen, M. *et al.* The RCP greenhouse gas concentrations and their extensions from 1765  
585 to 2300. *Clim. Change* **109**, 213-241, doi:10.1007/s10584-011-0156-z (2011).
- 586 34 Hurst, M. D., Rood, D. H., Ellis, M. A., Anderson, R. S. & Dornbusch, U. Recent acceleration in  
587 coastal cliff retreat rates on the south coast of Great Britain. *Proceedings of the National*  
588 *Academy of Sciences* **113**, 13336-13341, doi:10.1073/pnas.1613044113 (2016).
- 589 35 Ruggiero, P. Is the Intensifying Wave Climate of the U.S. Pacific Northwest Increasing Flooding  
590 and Erosion Risk Faster Than Sea-Level Rise? *Journal of Waterway, Port, Coastal, and Ocean*  
591 *Engineering* **139**, 88-97, doi:doi:10.1061/(ASCE)WW.1943-5460.0000172 (2013).
- 592 36 Loureiro, C., Ferreira, Ó. & Cooper, J. A. G. Extreme erosion on high-energy embayed beaches:  
593 Influence of megarrips and storm grouping. *Geomorphology* **139–140**, 155-171,  
594 doi:http://dx.doi.org/10.1016/j.geomorph.2011.10.013 (2012).
- 595 37 Kroon, A. *et al.* Statistical analysis of coastal morphological data sets over seasonal to decadal  
596 time scales. *Coastal Eng.* **55**, 581-600 (2008).
- 597 38 Gallop, S. L., Bosserelle, C., Pattiaratchi, C. & Eliot, I. Rock topography causes spatial variation in  
598 the wave, current and beach response to sea breeze activity. *Mar. Geol.* **290**, 29-40,  
599 doi:10.1016/j.margeo.2011.10.002 (2011).
- 600 39 Vousdoukas, M. I., Velegrakis, A. F. & Plomaritis, T. A. Beachrock occurrence, characteristics,  
601 formation mechanisms and impacts. *Earth-Science Reviews* **85**, 23-46,  
602 doi:10.1016/j.earscirev.2007.07.002 (2007).
- 603 40 Vousdoukas, M. I., Almeida, L. P. & Ferreira, Ó. Beach erosion and recovery during consecutive  
604 storms at a steep-sloping, meso-tidal beach. *Earth Surf. Processes Landforms* **37**, 583-691,  
605 doi:10.1002/esp.2264 (2012).
- 606 41 Ranasinghe, R., Callaghan, D. & Stive, M. J. F. Estimating coastal recession due to sea level rise:  
607 beyond the Bruun rule. *Clim. Change* **110**, 561-574, doi:10.1007/s10584-011-0107-8 (2012).
- 608 42 Coco, G. *et al.* Beach response to a sequence of extreme storms. *Geomorphology* **204**, 493-501,  
609 doi:http://dx.doi.org/10.1016/j.geomorph.2013.08.028 (2014).
- 610 43 Hardisty, J. in *Sediment Transport and Depositional Processes* (ed K. Pye)216-255 (Blackwell,  
611 1994).
- 612 44 Pekel, J.-F., Cottam, A., Gorelick, N. & Belward, A. S. High-resolution mapping of global surface  
613 water and its long-term changes. *Nature* **540**, 418, doi:10.1038/nature20584  
614 <https://www.nature.com/articles/nature20584#supplementary-information> (2016).
- 615 45 Haklay, M. & Weber, P. OpenStreetMap: User-Generated Street Maps. *IEEE Pervasive*  
616 *Computing* **7**, 12-18, doi:10.1109/MPRV.2008.80 (2008).
- 617 46 Boak, E. H. & Turner, I. L. Shoreline Definition and Detection: A Review. *J. Coast. Res.*, 688-703,  
618 doi:doi:10.2112/03-0071.1 (2005).
- 619 47 Jackson, L. P. & Jevrejeva, S. A probabilistic approach to 21st century regional sea-level  
620 projections using RCP and High-end scenarios. *Global Planet. Change* **146**, 179-189,  
621 doi:http://dx.doi.org/10.1016/j.gloplacha.2016.10.006 (2016).
- 622 48 Yamazaki, D. *et al.* A high-accuracy map of global terrain elevations. *Geophys. Res. Lett.* **44**,  
623 5844-5853, doi:doi:10.1002/2017GL072874 (2017).

624 49 Weatherall, P. *et al.* A new digital bathymetric model of the world's oceans. *Earth and Space*  
625 *Science* **2**, 331-345, doi:doi:10.1002/2015EA000107 (2015).

626 50 Hallermeier, R. J. in *16th International Conference on Coastal Engineering*.1493-1512 (ASCE).

627 51 Nicholls, R. J., Birkemeier, W. A. & Lee, G.-h. Evaluation of depth of closure using data from  
628 Duck, NC, USA. *Mar. Geol.* **148**, 179-201 (1998).

629 52 Baron, H. M. *et al.* Incorporating climate change and morphological uncertainty into coastal  
630 change hazard assessments. *Nat. Hazards* **75**, 2081-2102, doi:10.1007/s11069-014-1417-8  
631 (2015).

632 53 Ranasinghe, R., Duong, T. M., Uhlenbrook, S., Roelvink, D. & Stive, M. Climate-change impact  
633 assessment for inlet-interrupted coastlines. *Nature Climate Change* **3**, 83,  
634 doi:10.1038/nclimate1664

635 <https://www.nature.com/articles/nclimate1664#supplementary-information> (2012).

636 54 Vousdoukas, M. I., Mentaschi, L., Voukouvalas, E., Verlaan, M. & Feyen, L. Extreme sea levels on  
637 the rise along Europe's coasts. *Earth's Future*, n/a-n/a, doi:10.1002/2016EF000505 (2017).

638 55 Queffelec, P. & Croizé-Fillon, D. Global altimeter SWH data set. (Laboratoire d'Océanographie  
639 Spatiale, IFREMER, 2014).

640 56 Li, F. *Probabilistic estimation of dune erosion and coastal zone risk* PhD Thesis thesis, Delft  
641 University of Technology, (2014).

642 57 Toimil, A., Losada, I. J., Camus, P. & Díaz-Simal, P. Managing coastal erosion under climate  
643 change at the regional scale. *Coastal Eng.* **128**, 106-122,  
644 doi:<https://doi.org/10.1016/j.coastaleng.2017.08.004> (2017).

645 58 Le Cozannet, G. *et al.* Quantifying uncertainties of sandy shoreline change projections as sea  
646 level rises. *Scientific Reports* **9**, 42, doi:10.1038/s41598-018-37017-4 (2019).

647 59 Lentz, E. E. *et al.* Evaluation of dynamic coastal response to sea-level rise modifies inundation  
648 likelihood. *Nature Clim. Change* **6**, 696–700, doi:10.1038/nclimate2957

649 [http://www.nature.com/nclimate/journal/vaop/ncurrent/abs/nclimate2957.html#supplementary-](http://www.nature.com/nclimate/journal/vaop/ncurrent/abs/nclimate2957.html#supplementary-information)  
650 [information](http://www.nature.com/nclimate/journal/vaop/ncurrent/abs/nclimate2957.html#supplementary-information) (2016).

651 60 Jagers, B. R., J. L.; Verlaan, M.; Lalic, A.; Genseberger, M.; Friocourt, Y.; van der Pijl, S. in  
652 *American Geophysical Union, Fall Meeting 2014*(San Francisco, USA, 2014).

653 61 Muis, S., Verlaan, M., Winsemius, H. C., Aerts, J. C. J. H. & Ward, P. J. A global reanalysis of storm  
654 surges and extreme sea levels. *Nat Commun* **7**, doi:10.1038/ncomms11969 (2016).

655 62 US Army Corps of Engineers. *Coastal Engineering Manual*.(U.S. Army Corps of Engineers, 2002).

656 63 Mentaschi, L. *et al.* Non-stationary Extreme Value Analysis: a simplified approach for Earth  
657 science applications. *Hydrol. Earth Syst. Sci. Discuss.* **2016**, 1-38, doi:10.5194/hess-2016-65  
658 (2016).

659 64 Corbane, C. *et al.* Big earth data analytics on Sentinel-1 and Landsat imagery in support to global  
660 human settlements mapping. *Big Earth Data* **1**, 118-144, doi:10.1080/20964471.2017.1397899  
661 (2017).

662 65 IPCC. *Managing the Risks of Extreme Events and Disasters to Advance Climate Change*  
663 *Adaptation. A Special Report of Working Groups I and II of the Intergovernmental Panel on*  
664 *Climate Change*.(Cambridge University Press, 2012).

665 66 Antolínez, J. A. A. *et al.* A multiscale climate emulator for long-term morphodynamics (MUSCLE-  
666 morpho). *Journal of Geophysical Research: Oceans* **121**, 775-791, doi:doi:10.1002/2015JC011107  
667 (2016).

668 67 Enríquez, A. R., Marcos, M., Álvarez-Ellacuría, A., Orfila, A. & Gomis, D. Changes in beach  
669 shoreline due to sea level rise and waves under climate change scenarios: application to the

670 Balearic Islands (western Mediterranean). *Nat. Hazards Earth Syst. Sci.* **17**, 1075-1089,  
671 doi:10.5194/nhess-17-1075-2017 (2017).

672 68 Anderson, D., Ruggiero, P., Antolínez, J. A. A., Méndez, F. J. & Allan, J. A Climate Index Optimized  
673 for Longshore Sediment Transport Reveals Interannual and Multidecadal Littoral Cell Rotations.  
674 *Journal of Geophysical Research: Earth Surface* **123**, 1958-1981, doi:10.1029/2018JF004689  
675 (2018).

676 69 Giardino, A. *et al.* A quantitative assessment of human interventions and climate change on the  
677 West African sediment budget. *Ocean Coast. Manag.* **156**, 249-265,  
678 doi:https://doi.org/10.1016/j.ocecoaman.2017.11.008 (2018).

679 70 Vitousek, S., Barnard, P. L., Limber, P., Erikson, L. & Cole, B. A model integrating longshore and  
680 cross-shore processes for predicting long-term shoreline response to climate change. *Journal of*  
681 *Geophysical Research: Earth Surface* **122**, 782-806, doi:10.1002/2016jf004065 (2017).

682 71 Wainwright, D. J. *et al.* Moving from deterministic towards probabilistic coastal hazard and risk  
683 assessment: Development of a modelling framework and application to Narrabeen Beach, New  
684 South Wales, Australia. *Coastal Eng.* **96**, 92-99,  
685 doi:https://doi.org/10.1016/j.coastaleng.2014.11.009 (2015).

686 72 Ranasinghe, R. & Stive, M. J. F. Rising seas and retreating coastlines. *Clim. Change* **97**, 465,  
687 doi:10.1007/s10584-009-9593-3 (2009).

688 73 Davidson, M. A., Splinter, K. D. & Turner, I. L. A simple equilibrium model for predicting shoreline  
689 change. *Coastal Eng.* **73**, 191-202, doi:http://dx.doi.org/10.1016/j.coastaleng.2012.11.002  
690 (2013).

691 74 Ozkan-Haller, T., Brundidge, S. Equilibrium Beach Profiles for Delaware Beaches. 147-160 (2007).

692 75 Cooper, J. A. G. & Pilkey, O. H. Sea-level rise and shoreline retreat: time to abandon the Bruun  
693 Rule. *Global Planet. Change* **43**, 157-171, doi:http://dx.doi.org/10.1016/j.gloplacha.2004.07.001  
694 (2004).

695 76 Pilkey, O. H. & Dixon, K. L. *The Corps and the Shore*. (Island Press, 1996).

696 77 Pilkey, O. H. *et al.* The Concept of Shoreface Profile of Equilibrium: A Critical Review. *Journal of*  
697 *Coastal Research SI* **9**, 225-278 (1993).

698 78 Holman, R. A., Lalejini, D. M., Edwards, K. & Veeramony, J. A parametric model for barred  
699 equilibrium beach profiles. *Coastal Eng.* **90**, 85-94,  
700 doi:http://dx.doi.org/10.1016/j.coastaleng.2014.03.005 (2014).

701 79 Coco, G. & Murray, A. B. Patterns in the sand: From forcing templates to self-organization.  
702 *Geomorphology* **91**, 271-290, doi:10.1016/j.geomorph.2007.04.023 (2007).

703 80 Voudoukas, M. I. Erosion/accretion and multiple beach cusp systems on a meso-tidal, steeply-  
704 sloping beach. *Geomorphology* **141-142**, 34-46, doi:doi:10.1016/j.geomorph.2011.12.003  
705 (2012).

706 81 Wang, Z. & Dean, R. G. in *Coastal Sediments '07* 626-632 (American Society of Civil Engineers,  
707 2007).

708 82 Dai, Z.-J., Du, J.-z., Li, C.-C. & Chen, Z.-S. The configuration of equilibrium beach profile in South  
709 China. *Geomorphology* **86**, 441-454, doi:http://dx.doi.org/10.1016/j.geomorph.2006.09.016  
710 (2007).

711 83 Romanczyk, W., Boczar-Karakiewicz, B. & Bona, J. L. Extended equilibrium beach profiles.  
712 *Coastal Eng.* **52**, 727-744, doi:https://doi.org/10.1016/j.coastaleng.2005.05.002 (2005).

713 84 Anderson, T. R., Fletcher, C. H., Barbee, M. M., Frazer, L. N. & Romine, B. M. Doubling of coastal  
714 erosion under rising sea level by mid-century in Hawaii. *Nat. Hazards* **78**, 75-103,  
715 doi:10.1007/s11069-015-1698-6 (2015).

716 85 Bray, M. & Hooke, J. Prediction of soft-cliff retreat with accelerating sea-level rise. *J. Coast. Res.*  
717 **13**, 453-467 (1997).

718 86 Pilkey, O. H. & Cooper, J. A. G. Society and Sea Level Rise. *Science* **303**, 1781,  
719 doi:10.1126/science.1093515 (2004).

720 87 Splinter, K. D., Carley, J. T., Golshani, A. & Tomlinson, R. A relationship to describe the  
721 cumulative impact of storm clusters on beach erosion. *Coastal Eng.* **83**, 49-55,  
722 doi:http://dx.doi.org/10.1016/j.coastaleng.2013.10.001 (2014).

723 88 Vousdoukas, M. I., Ferreira, O., Almeida, L. P. & Pacheco, A. Toward reliable storm-hazard  
724 forecasts: XBeach calibration and its potential application in an operational early-warning  
725 system. *Ocean Dyn.* **62**, 1001-1015, doi:10.1007/s10236-012-0544-6 (2012).

726 89 Roelvink, D. *et al.* Modelling storm impacts on beaches, dunes and barrier islands. *Coastal Eng.*  
727 **56**, 1133-1152 (2009).

728 90 Broekema, Y. B. *et al.* Observations and modelling of nearshore sediment sorting processes  
729 along a barred beach profile. *Coastal Eng.* **118**, 50-62,  
730 doi:https://doi.org/10.1016/j.coastaleng.2016.08.009 (2016).

731 91 de Winter, R. C. & Ruessink, B. G. Sensitivity analysis of climate change impacts on dune erosion:  
732 case study for the Dutch Holland coast. *Clim. Change* **141**, 685-701, doi:10.1007/s10584-017-  
733 1922-3 (2017).

734 92 Karunaratna, H., Brown, J., Chatzirodou, A., Dissanayake, P. & Wisse, P. Multi-timescale  
735 morphological modelling of a dune-fronted sandy beach. *Coastal Eng.* **136**, 161-171,  
736 doi:https://doi.org/10.1016/j.coastaleng.2018.03.005 (2018).

737 93 Passeri, D. L., Bilskie, M. V., Plant, N. G., Long, J. W. & Hagen, S. C. Dynamic modeling of barrier  
738 island response to hurricane storm surge under future sea level rise. *Clim. Change* **149**, 413-425,  
739 doi:10.1007/s10584-018-2245-8 (2018).

740 94 Callaghan, D. P., Nielsen, P., Short, A. D. & Ranasinghe, R. Statistical simulation of wave climate  
741 and extreme beach erosion. *Coastal Eng.* **55**, 375-390 (2008).

742 95 Ferreira, Ó., Garcia, T., Matias, A., Taborde, R. & Dias, J. A. An integrated method for the  
743 determination of set-back lines for coastal erosion hazards on sandy shores. *Cont. Shelf Res.* **26**,  
744 1030-1044 (2006).

745 96 Mull, J. & Ruggiero, P. Estimating Storm-Induced Dune Erosion and Overtopping along U.S. West  
746 Coast Beaches. *J. Coast. Res.*, 1173-1187, doi:10.2112/JCOASTRES-D-13-00178.1 (2014).

747 97 Ferreira, Ó. Storm groups versus extreme single storms: Predicted erosion and management  
748 consequences. *Journal of Coastal Research* **42**, 155-161 (2005).

749 98 Dissanayake, P., Brown, J. & Karunaratna, H. Impacts of storm chronology on the  
750 morphological changes of the Formby beach and dune system, UK. *Nat. Hazards Earth Syst. Sci.*  
751 *Discuss.* **3**, 2565-2597, doi:10.5194/nhessd-3-2565-2015 (2015).

752 99 Hackney, C., Darby, S. E. & Leyland, J. Modelling the response of soft cliffs to climate change: A  
753 statistical, process-response model using accumulated excess energy. *Geomorphology* **187**, 108-  
754 121, doi:https://doi.org/10.1016/j.geomorph.2013.01.005 (2013).

755 100 Yates, M. L., Guza, R. T. & O'Reilly, W. C. Equilibrium shoreline response: Observations and  
756 modeling. *Journal of Geophysical Research C: Oceans* **114** (2009).

757 101 Pontee, N. Defining coastal squeeze: A discussion. *Ocean Coast. Manag.* **84**, 204-207,  
758 doi:https://doi.org/10.1016/j.ocecoaman.2013.07.010 (2013).

759 102 Doody, J. P. Coastal squeeze and managed realignment in southeast England, does it tell us  
760 anything about the future? *Ocean Coast. Manag.* **79**, 34-41,  
761 doi:https://doi.org/10.1016/j.ocecoaman.2012.05.008 (2013).

762 103 Monioudi, I. N. *et al.* Assessment of island beach erosion due to sea level rise: the case of the  
763 Aegean archipelago (Eastern Mediterranean). *Nat. Hazards Earth Syst. Sci.* **17**, 449-466,  
764 doi:10.5194/nhess-17-449-2017 (2017).

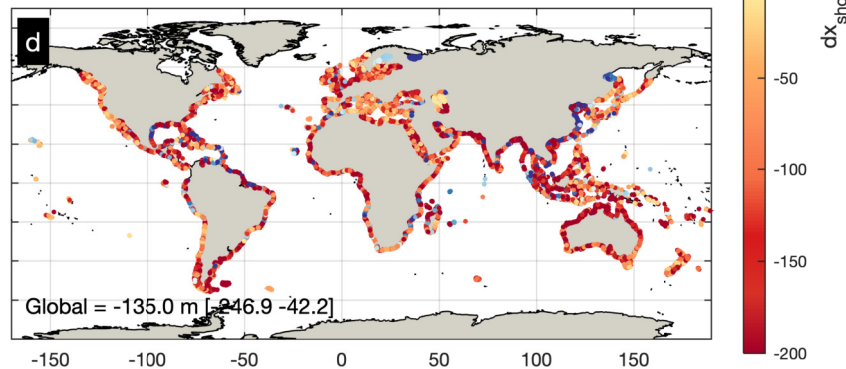
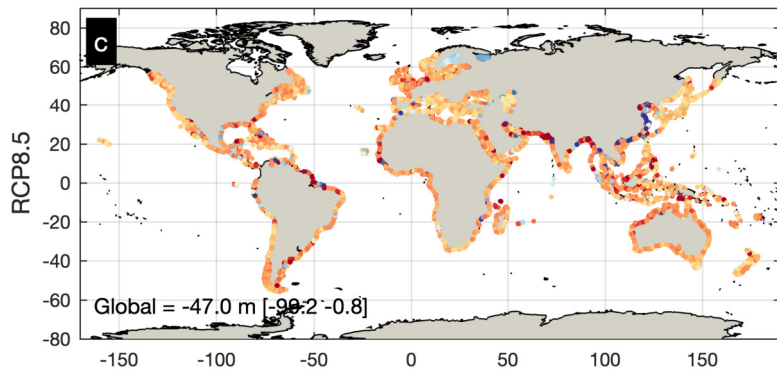
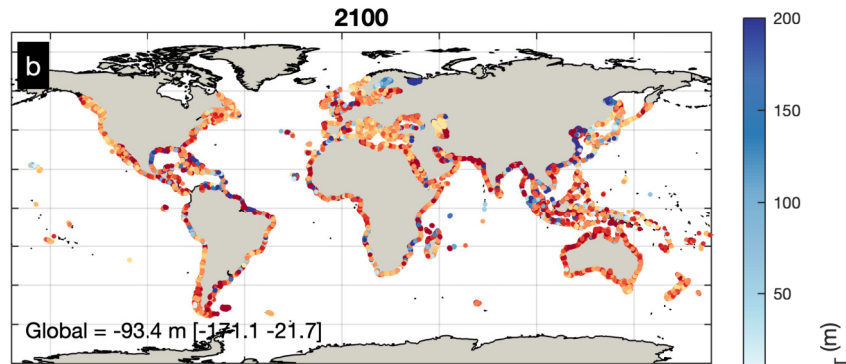
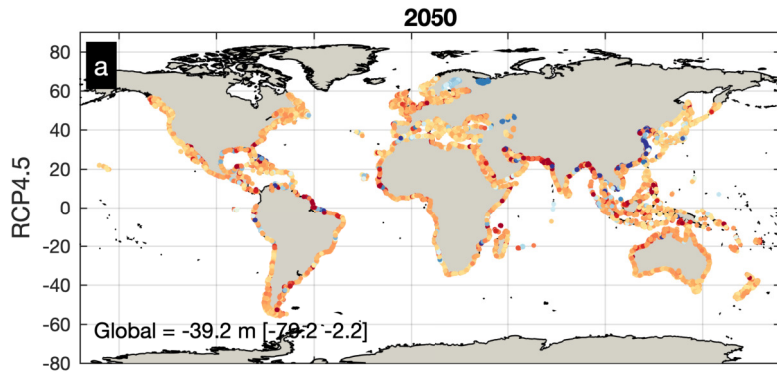
- 765 104 Rosen, T. & Xu, Y. J. Recent decadal growth of the Atchafalaya River Delta complex: Effects of  
766 variable riverine sediment input and vegetation succession. *Geomorphology* **194**, 108-120,  
767 doi:<https://doi.org/10.1016/j.geomorph.2013.04.020> (2013).
- 768 105 Peduzzi, P. *et al.* Global trends in tropical cyclone risk. *Nature Clim. Change* **2**, 289-294,  
769 doi:[http://www.nature.com/nclimate/journal/v2/n4/abs/nclimate1410.html#supplementary-](http://www.nature.com/nclimate/journal/v2/n4/abs/nclimate1410.html#supplementary-information)  
770 information (2012).
- 771 106 Travis, J. Scientists's Fears Come True as Hurricane Floods New Orleans. *Science* **309**, 1656,  
772 doi:10.1126/science.309.5741.1656 (2005).
- 773 107 Monteiro, M. C., Pereira, L. C. C. & de Oliveira, S. M. O. Morphodynamic Changes of a Macrotidal  
774 Sand Beach in the Brazilian Amazon Coast (Ajuruteua-Pará). *J. Coast. Res.*, 103-107 (2009).
- 775 108 Salomon, J.-N. L'accrétion littorale sur la côte Ouest de Madagascar. *Physio-Géo* **3**,  
776 doi:10.4000/physio-geo.671 (2009).
- 777 109 Taft, L. & Evers, M. A review of current and possible future human–water dynamics in  
778 Myanmar's river basins. *Hydrol. Earth Syst. Sci.* **20**, 4913-4928, doi:10.5194/hess-20-4913-2016  
779 (2016).
- 780 110 Marfai, M. A. & King, L. Monitoring land subsidence in Semarang, Indonesia. *Environ. Geol.* **53**,  
781 651-659, doi:10.1007/s00254-007-0680-3 (2007).
- 782 111 Rodolfo, K. S. & Siringan, F. P. Global sea-level rise is recognised, but flooding from  
783 anthropogenic land subsidence is ignored around northern Manila Bay, Philippines. *Disasters* **30**,  
784 118-139, doi:10.1111/j.1467-9523.2006.00310.x (2006).

785

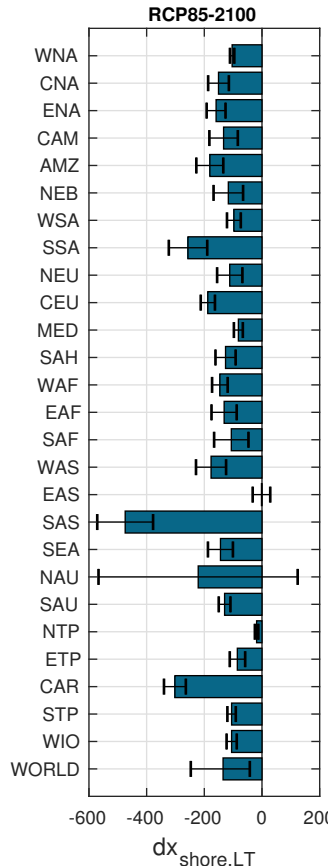
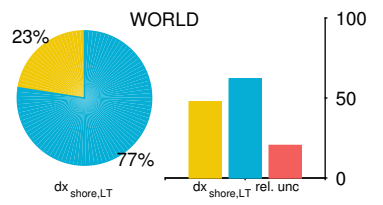
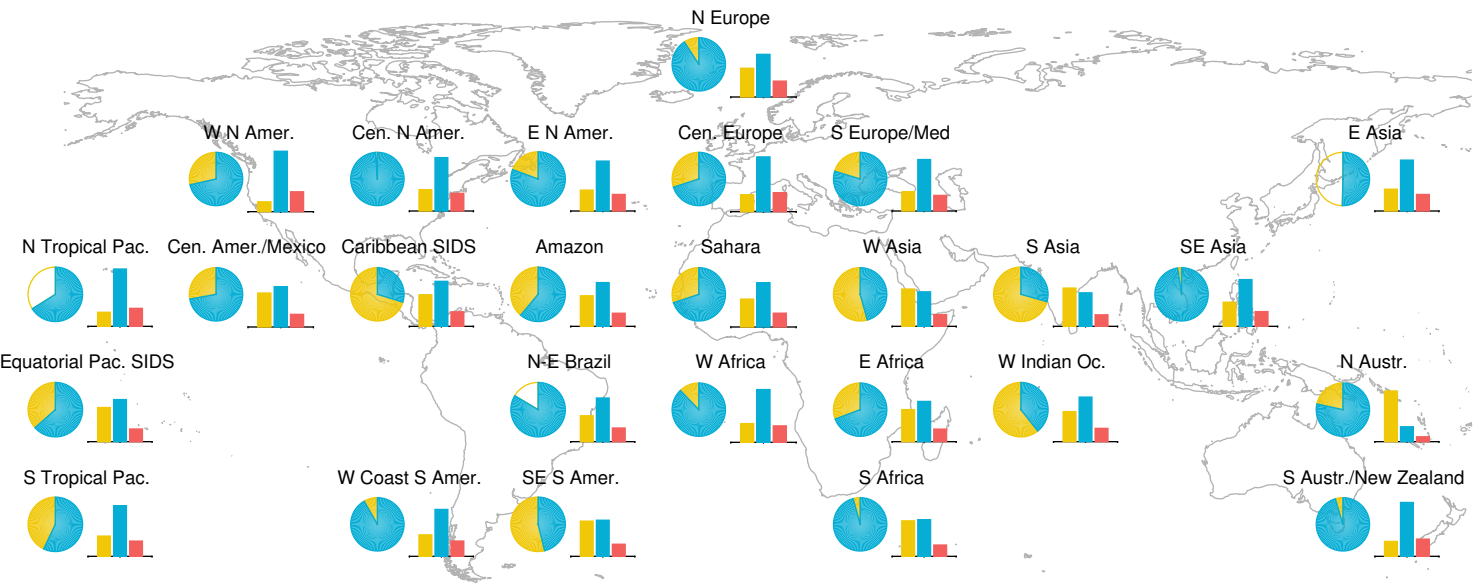
786

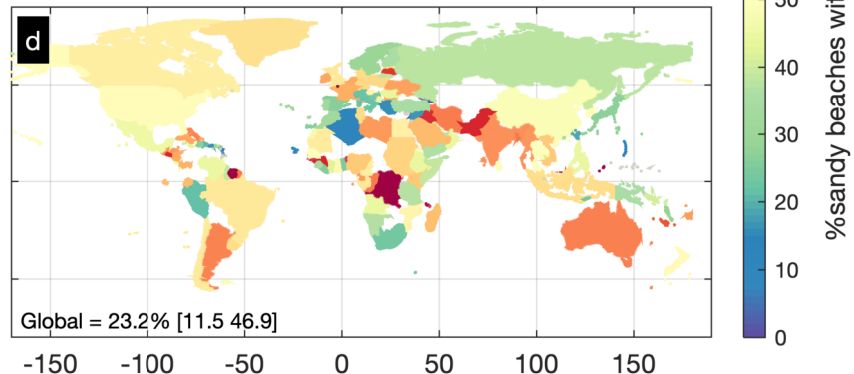
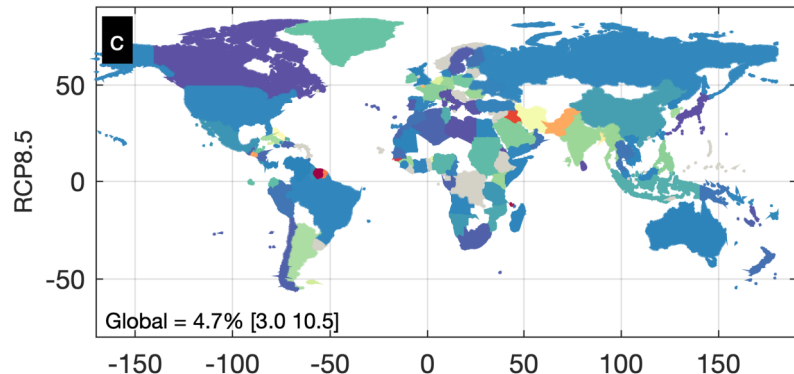
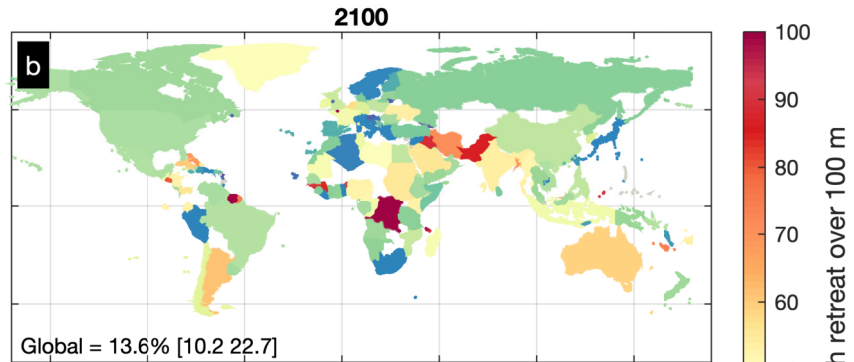
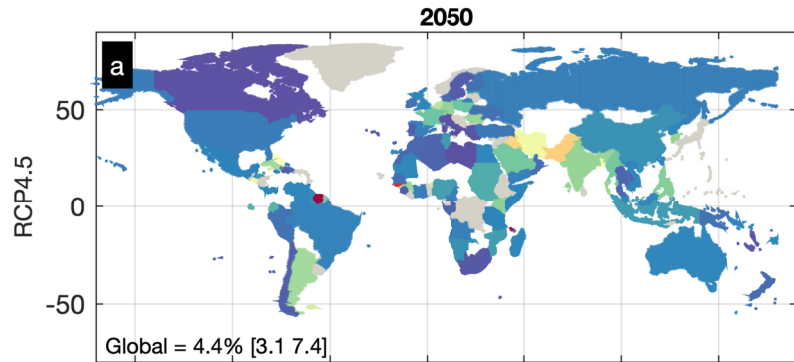
787

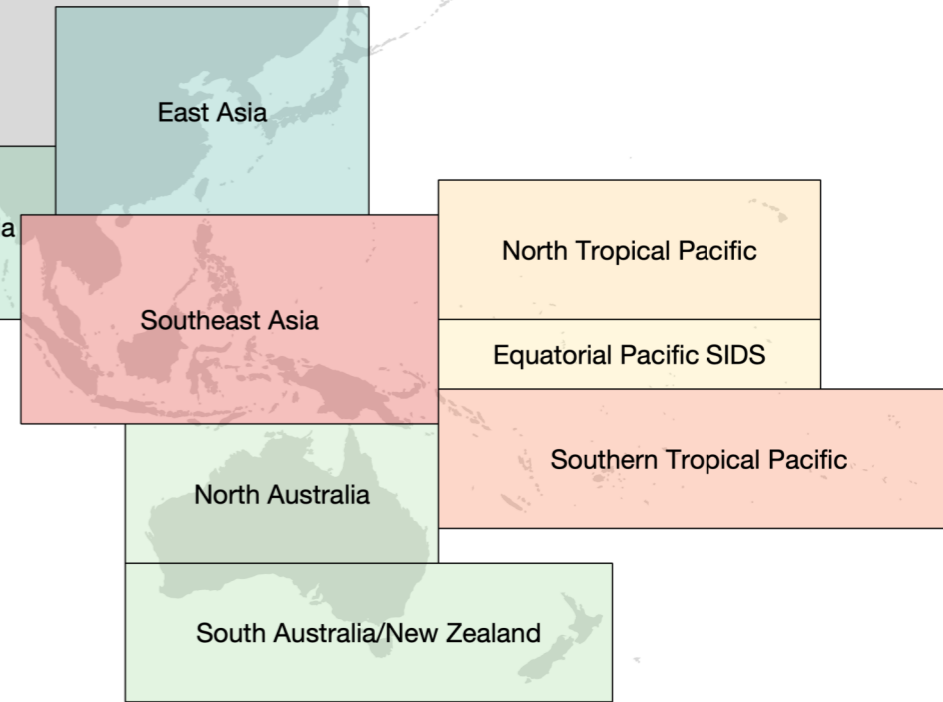
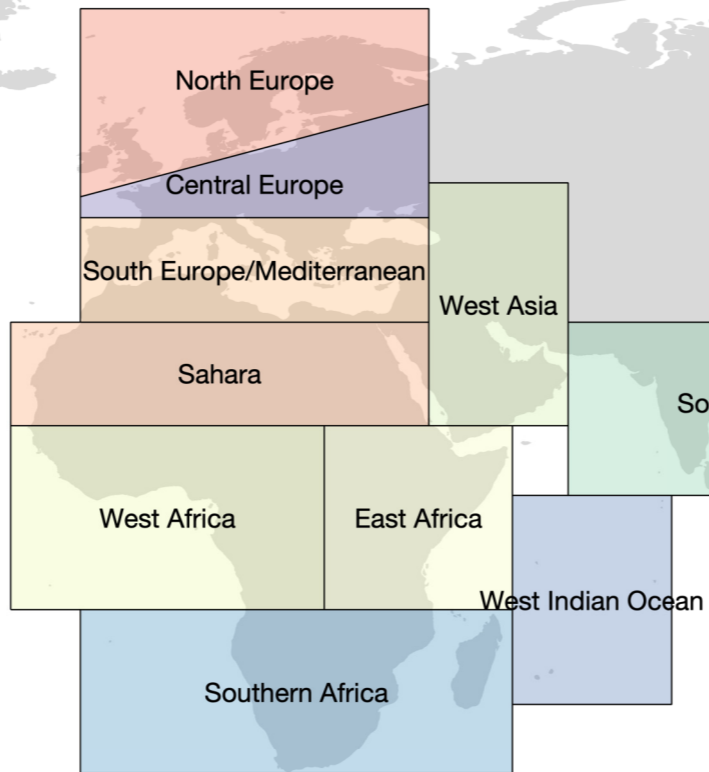
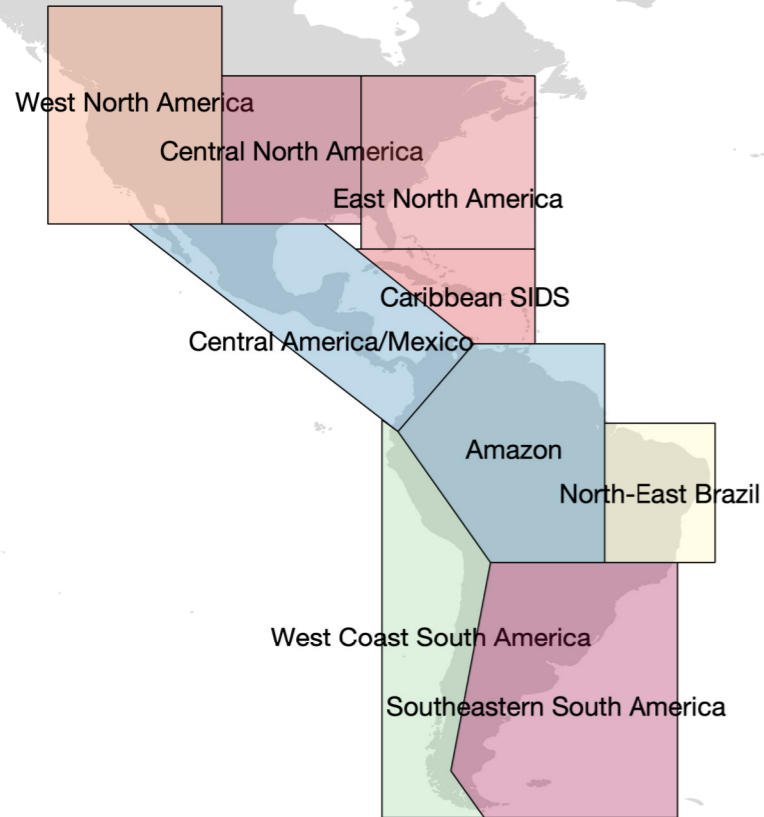


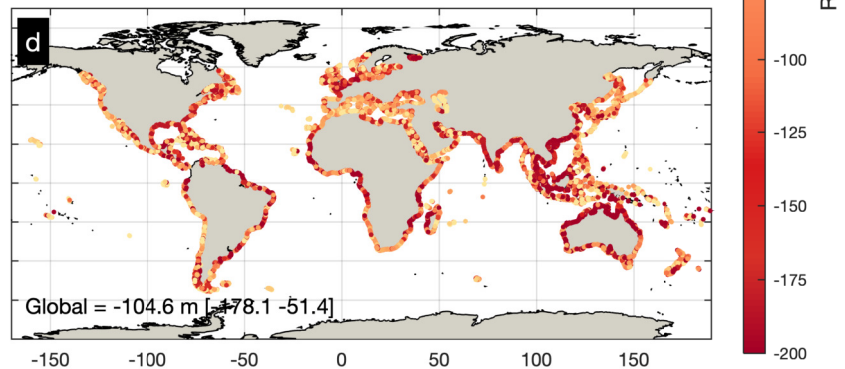
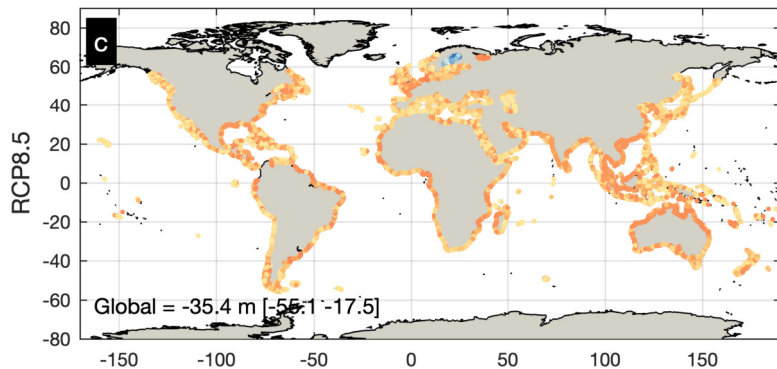
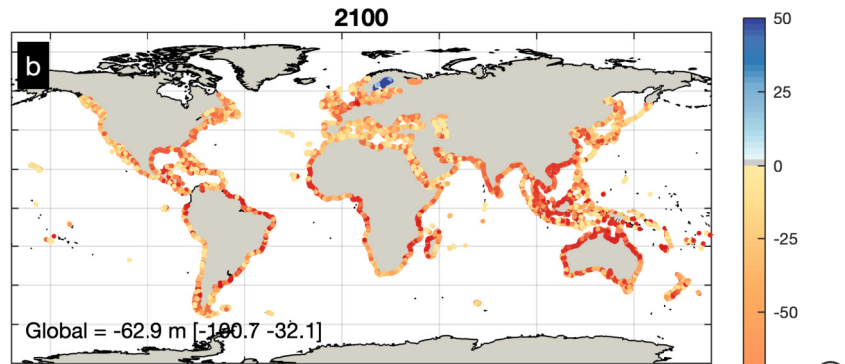
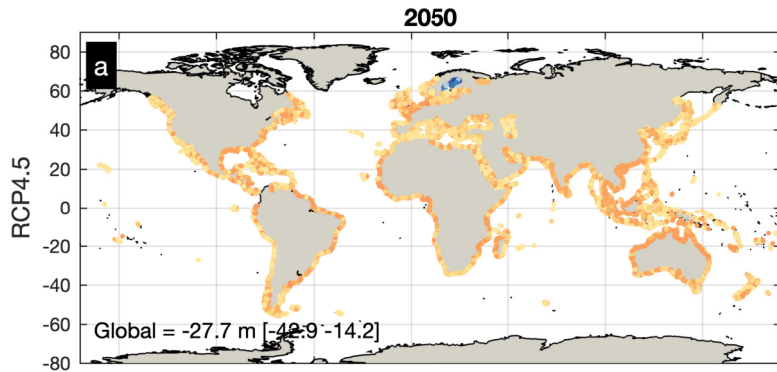


Ambient Change
  SLR Retreat
  RCP
  Shoreline Change

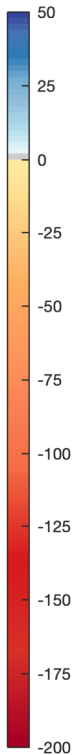




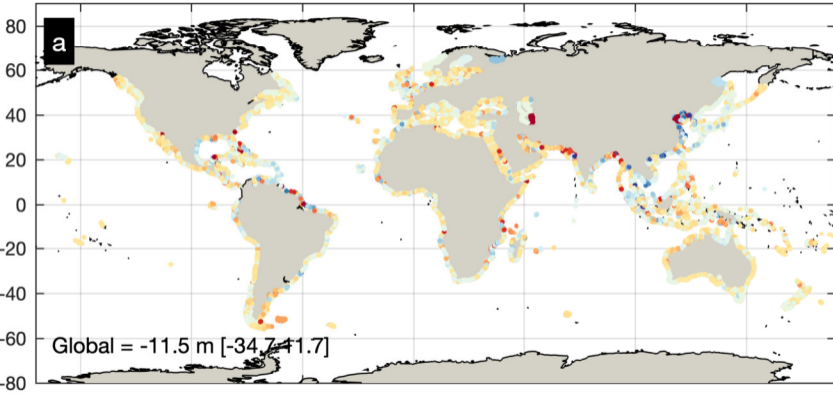




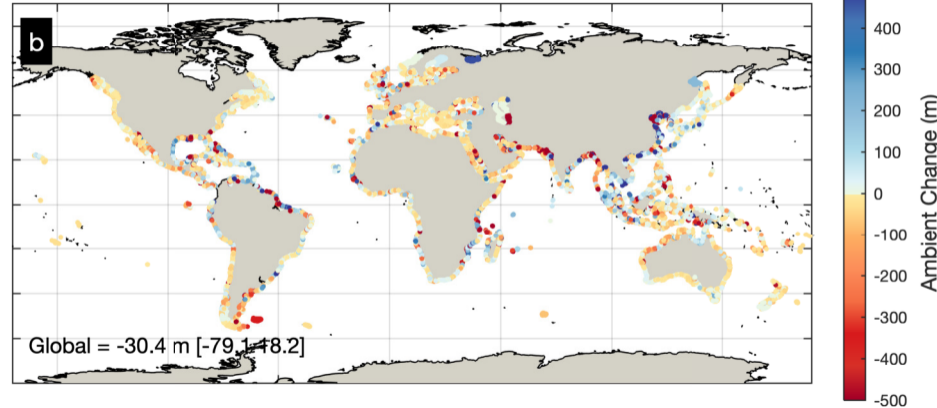
R (m)

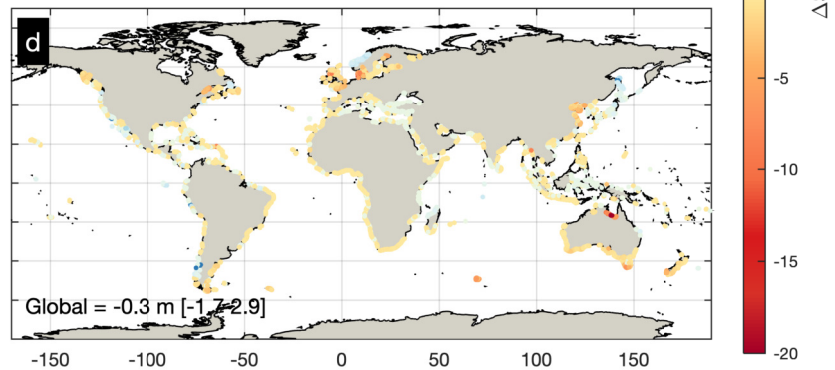
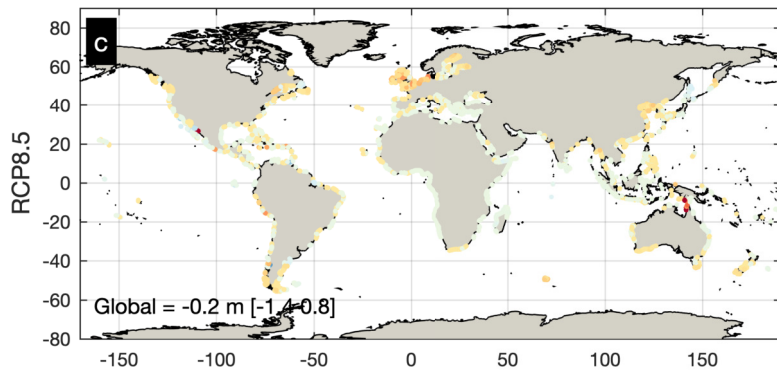
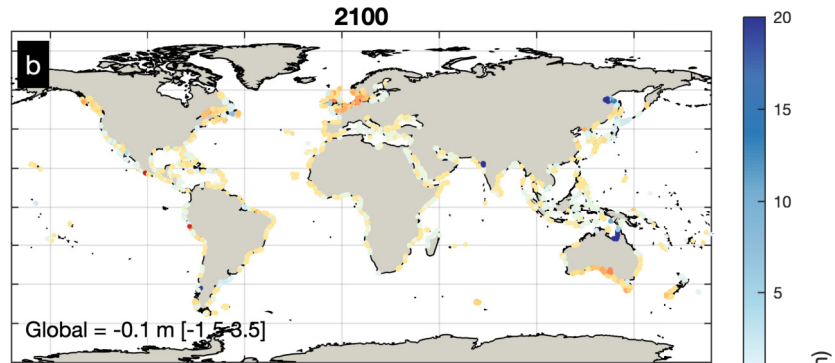
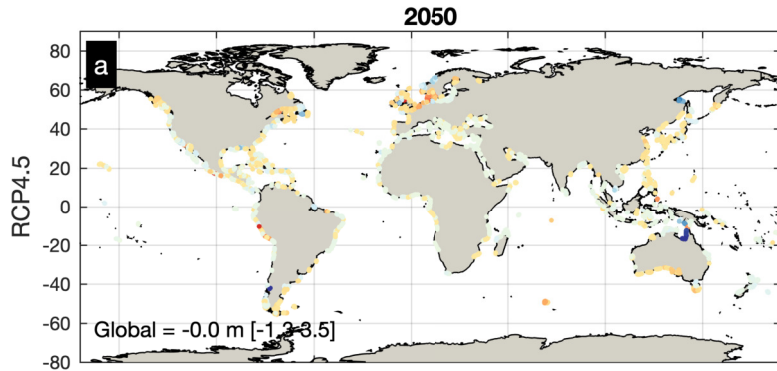


2050



2100





$\Delta S$  (m)

20

15

10

5

0

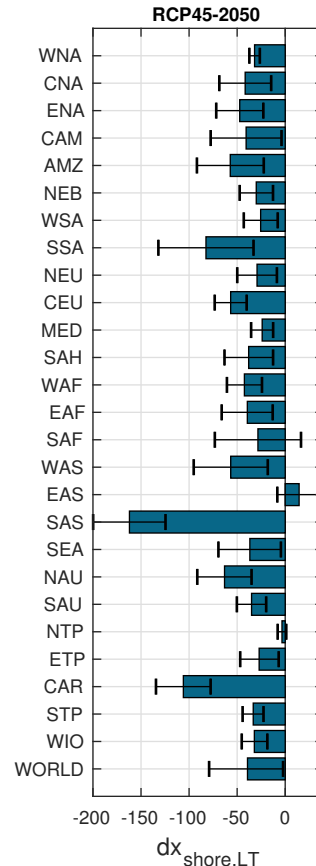
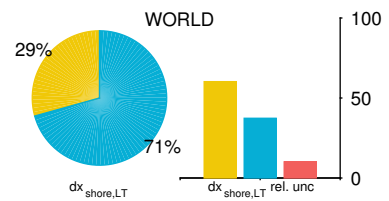
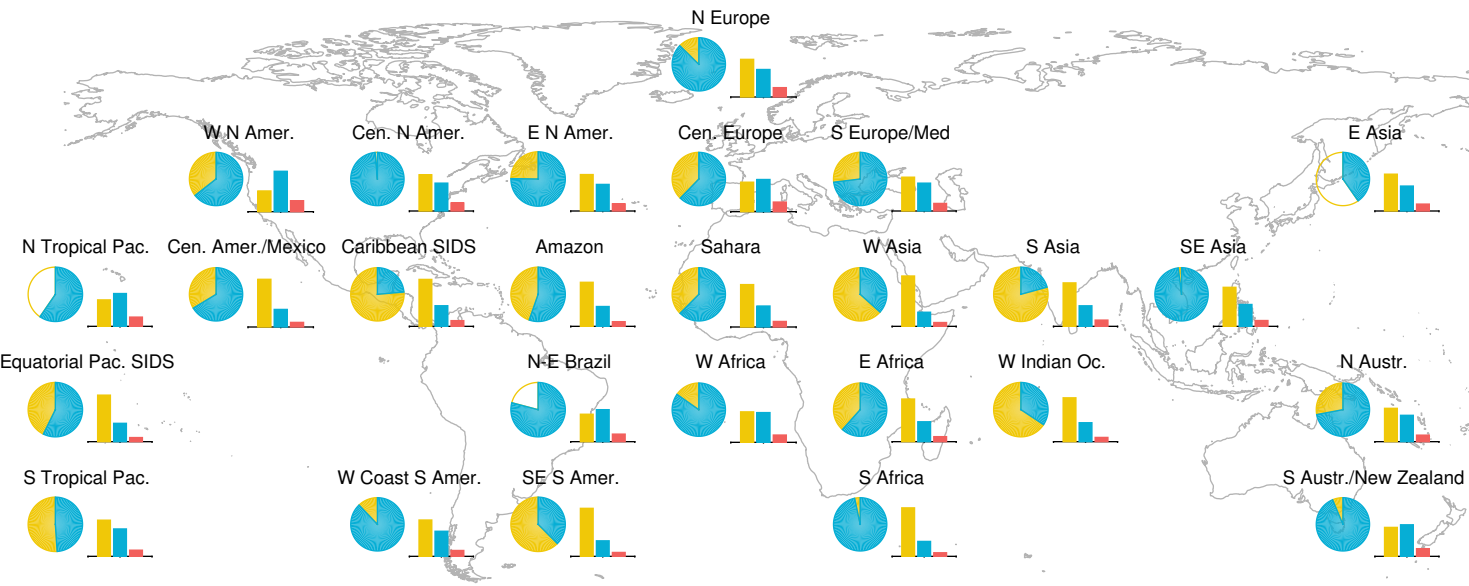
-5

-10

-15

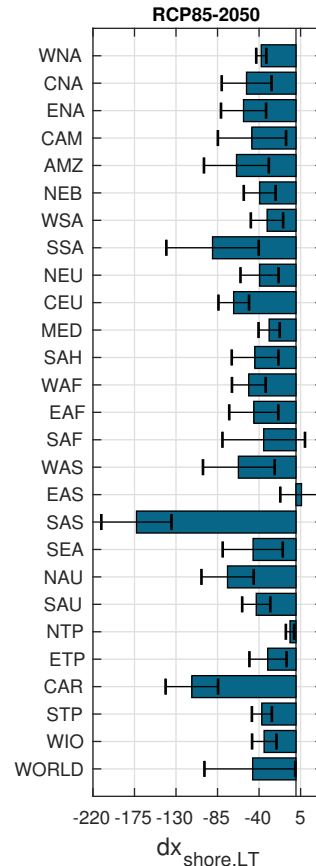
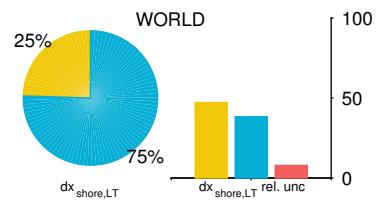
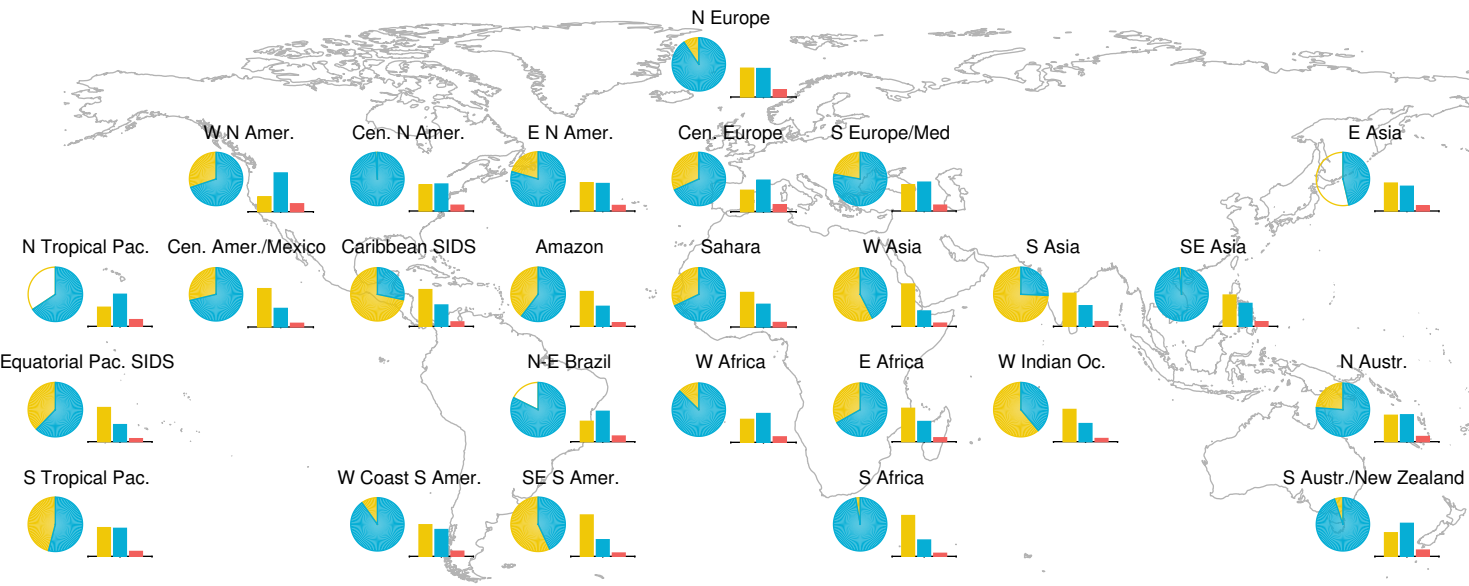
-20

Ambient Change
  SLR Retreat
  RCP
  Shoreline Change

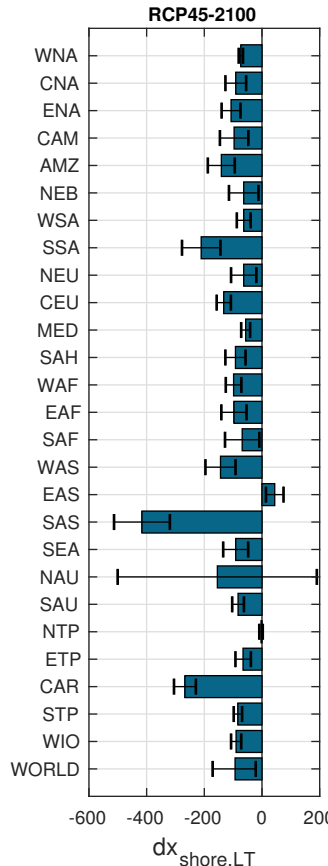
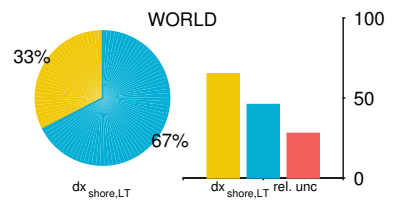
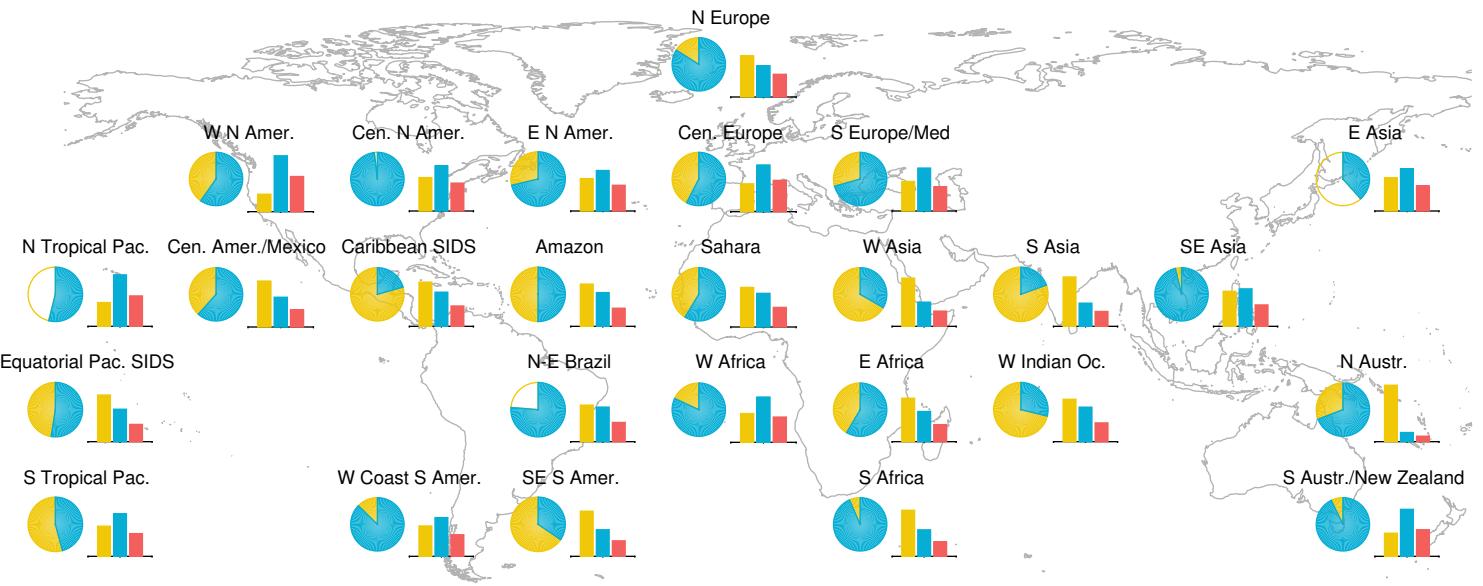




Ambient Change
  SLR Retreat
  RCP
  Shoreline Change

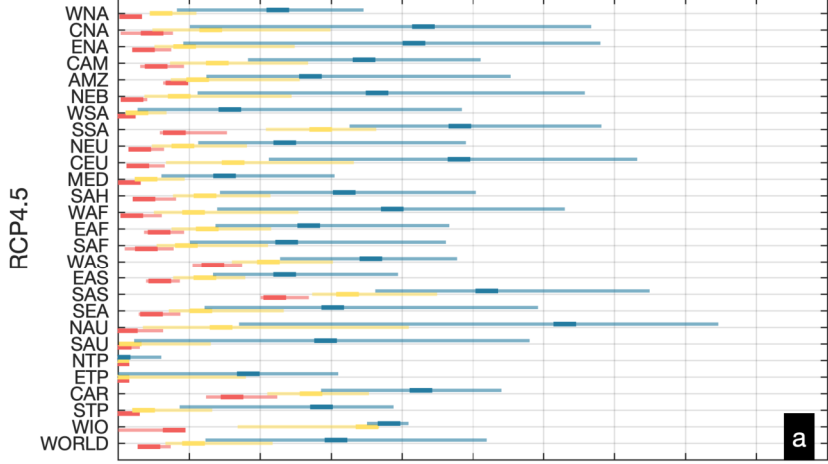


Ambient Change
  SLR Retreat
  RCP
  Shoreline Change

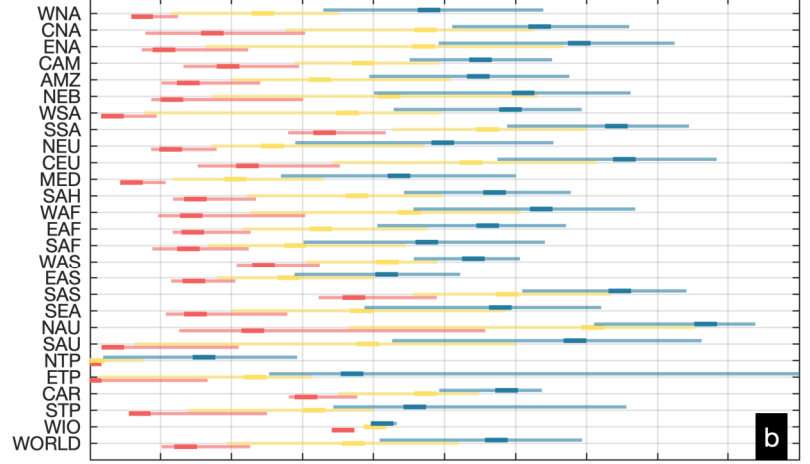


█  $dx_{shore} > 50$  m   
 █  $dx_{shore} > 100$  m   
 █  $dx_{shore} > 200$  m

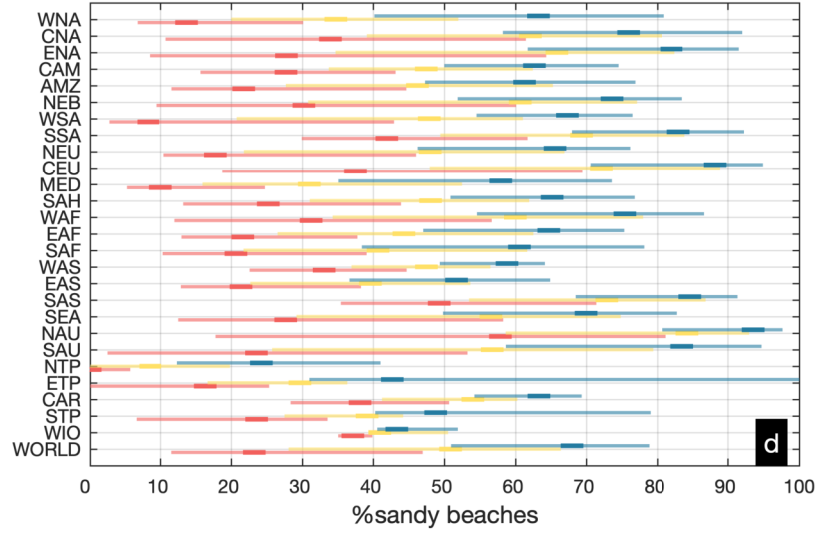
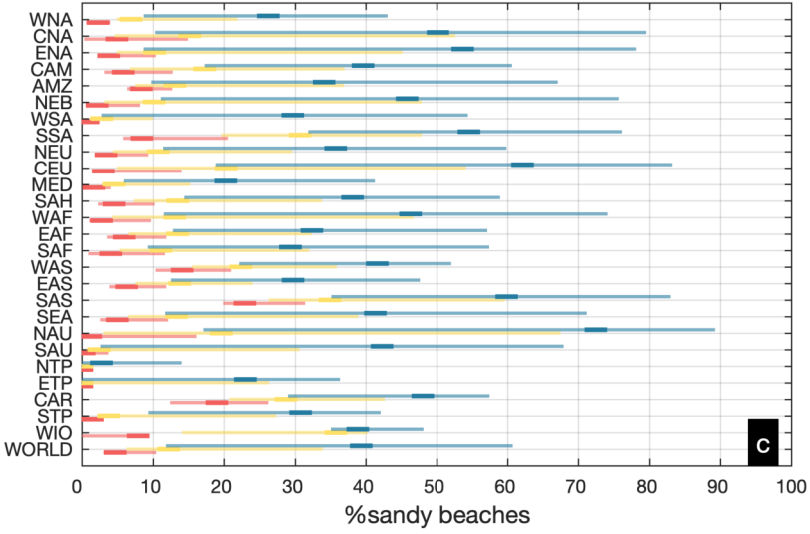
2050



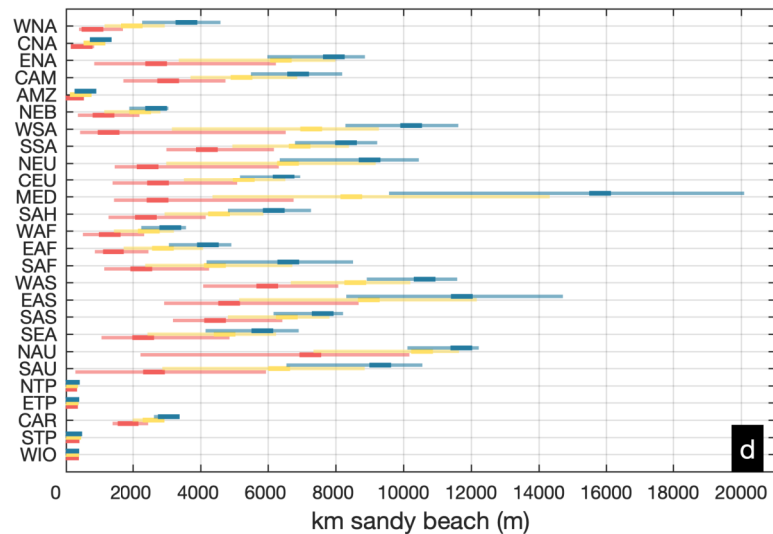
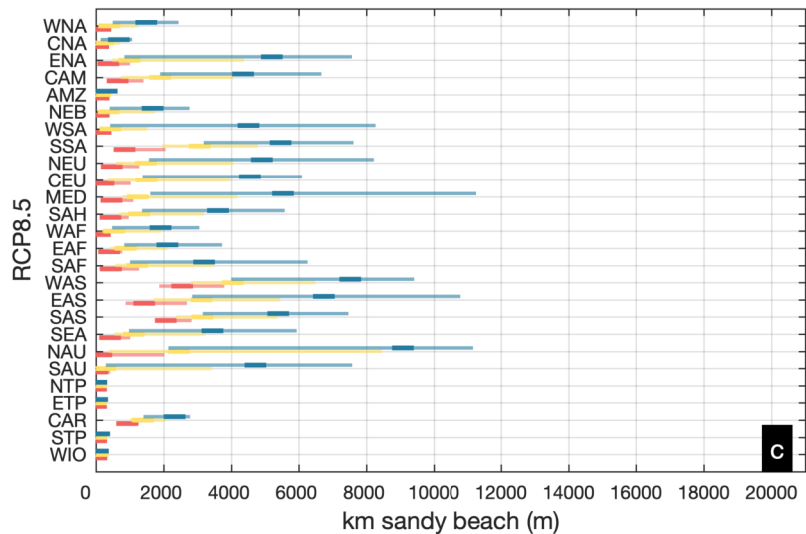
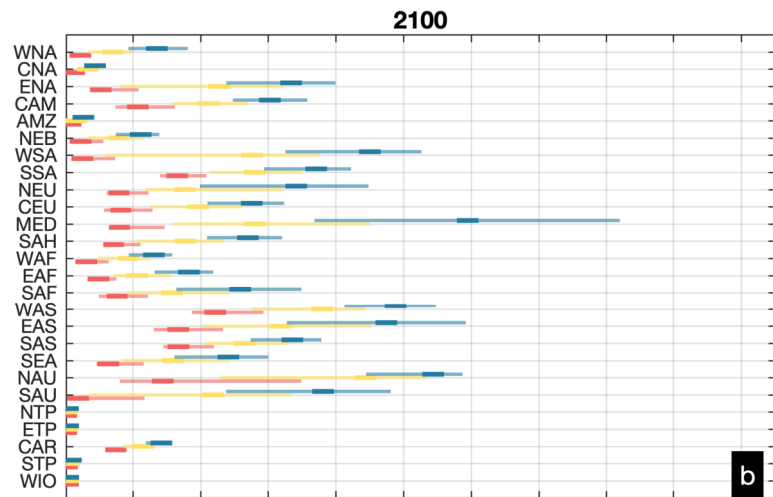
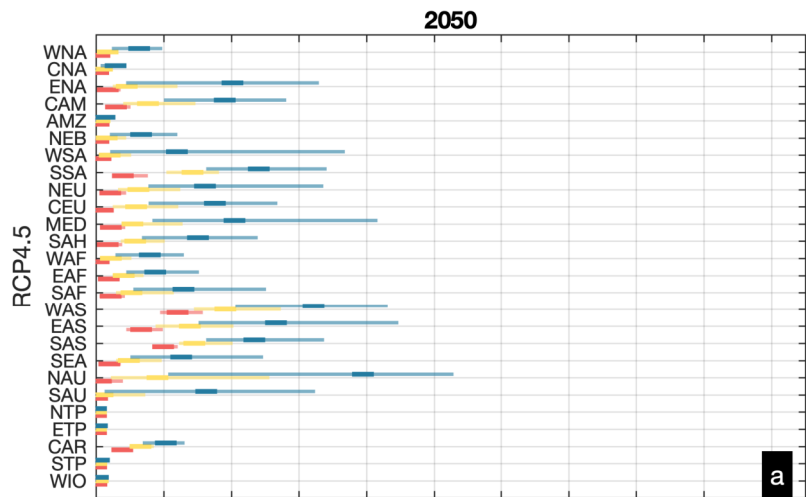
2100

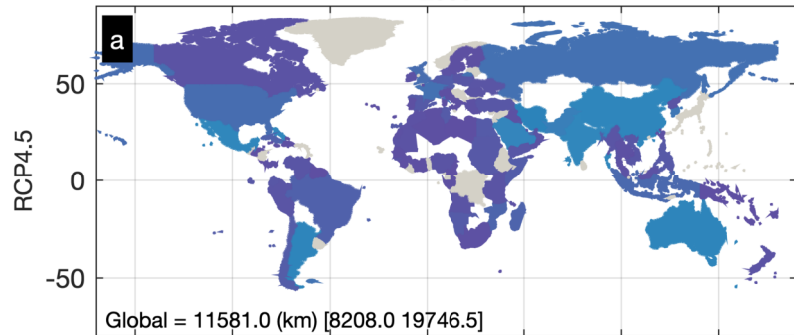


RCP8.5



■  $dx_{shore} > 50$  m   
 ■  $dx_{shore} > 100$  m   
 ■  $dx_{shore} > 200$  m



**2050****2100**